https://doi.org/10.5194/egusphere-2024-1750
Preprint. Discussion started: 20 June 2024

Ocean carbon sink assessment via temperature and salinity data assimilation into a global ocean biogeochemistry model

Frauke Bunsen[1], Judith Hauck[1], Lars Nerger[1], and Sinhué Torres-Valdés[1]

[1]Alfred-Wegener-Institut, Helmholtz Zentrum für Polar- und Meeresforschung, Bremerhaven, Germany

Correspondence: Frauke Bunsen (frauke.bunsen@awi.de)

Abstract. Global ocean biogeochemistry models are frequently used to derive a comprehensive estimate of the global ocean carbon uptake. These models are designed to represent the most important processes of the ocean carbon cycle, but the idealized process representation and uncertainties in the initialization of model variables lead to errors in their predictions. Here, observations of ocean physics (temperature and salinity) are assimilated into the ocean biogeochemistry model FESOM-REcoM over the period 2010-2020 to study the effect on the air-sea CO_2 flux and other biogeochemical variables. While the free running model already represents temperature and salinity rather well, the assimilation further improves it and hence influences the modeled ecosystem and CO_2 fluxes. The assimilation has mainly regional effects on the air-sea CO_2 flux, with the largest imprint of assimilation in the Southern Ocean during winter. South of $50\,°\mathrm{S}$, winter CO_2 outgassing is reduced and thus the mean CO_2 uptake increases by $0.18\,\mathrm{Pg\,C\,yr^{-1}}$ through the assimilation. Other particularly strong regional effects on the air-sea CO_2 flux are located in the area of the North Atlantic Current. Yet, the effect on the global ocean carbon uptake is a comparatively small increase by $0.05\,\mathrm{Pg\,C\,yr^{-1}}$ induced by the assimilation, yielding a global mean uptake of $2.78\,\mathrm{Pg\,C\,yr^{-1}}$ for the period 2010-2020.

1 Introduction

The ocean plays a pivotal role in regulating the global carbon budget and thereby mitigating the impacts of anthropogenic carbon dioxide (CO_2) emissions on the Earth's climate. Since the 1960s, the ocean has absorbed consistently around 25% of anthropogenic CO_2 emissions annually (Friedlingstein et al., 2023) and has cumulatively taken up 26–34% of fossil and land-use change CO2 emissions since the onset of the Industrial Revolution (Crisp et al., 2022). However, quantification of air-sea CO_2 flux still remains challenging. Air-sea CO2 flux is usually inferred from the gradient of partial pressure (pCO_2) or fugacity (fCO_2) of CO_2 across the air-sea interface (Wanninkhof, 2014). Yet, during 2010-2020, which constitutes the best-sampled decade in terms of surface ocean pCO_2 observations so far, observations covered merely 3% of the monthly global ocean (as calculated from the $1°$x$1°$-gridded SOCAT product; Bakker et al., 2016). While the North Atlantic and North Pacific are comparably well observed, data remain scarce in vast regions, such as the Indian Ocean, South Pacific and areas south

https://doi.org/10.5194/egusphere-2024-1750
Preprint. Discussion started: 20 June 2024

of 30°S during austral winter, where less than 1% of SOCAT grid cells have been sampled. Although these observations are thought to be representative of a larger area (Jones et al., 2012; Hauck et al., 2020), challenges in deriving a comprehensive global estimate of the global ocean CO_2 uptake arise due to substantial spatial and temporal pCO_2 variations and potential biases induced by the irregular sampling pattern (Denvil-Sommer et al., 2021; Gloege et al., 2021; Hauck et al., 2023b). Particularly in the Southern Ocean, the uncertainty is considerable (Gerber et al., 2009; Gloege et al., 2021), where estimates of the mean flux deviate by 14–26% (Hauck et al., 2023b).

Initially, estimates of the ocean carbon sink were derived from hindcast simulations of global ocean biogeochemistry models (GOBMs) (Le Quéré et al., 2009; Wanninkhof et al., 2013; Hauck et al., 2020). More recently, air-sea CO_2 flux estimates were added based on regression and machine learning techniques, interpolating pCO_2 observations to achieve global coverage through advanced statistical methods (referred to as pCO_2 products; Rödenbeck et al., 2015). Furthermore, atmospheric transport models that ingest atmospheric CO_2 measurements were employed to estimate the ocean carbon uptake (referred to as atmospheric inversions; Peylin et al., 2013). Although the different estimation methods have provided valuable and robust insights into large-scale patterns of oceanic carbon uptake (Gruber et al., 2009), discrepancies have emerged. Assessments based on pCO_2-products tend to yield larger estimates of the ocean carbon sink, with stronger trends towards more uptake, compared to estimates based on models (Friedlingstein et al., 2023; Terhaar et al., 2022). The larger estimates are supported by ocean interior observations (Müller et al., 2023), atmospheric oxygen data and atmospheric inversions (Friedlingstein et al., 2023). For the years 2010-2020, pCO_2 products suggest a mean oceanic sink of $(3.0 \pm 0.4)\,\mathrm{Pg\,C\,yr^{-1}}$, while the model mean is $(2.5 \pm 0.4)\,\mathrm{Pg\,C\,yr^{-1}}$, with trends of $0.7\,\mathrm{Pg\,C\,yr^{-1}\,dec^{-1}}$ and $0.3\,\mathrm{Pg\,C\,yr^{-1}\,dec^{-1}}$, respectively (data provided by Friedlingstein et al., 2023).

Machine learning estimates, on the one hand, perform better when trained with sufficient data, such as in the northern hemisphere (Gloege et al., 2021). However, as with other methods, their performance is less reliable in data-sparse areas. Particularly in the Southern Ocean, many pCO_2 products show diverging results from one another and are likely biased towards more ocean uptake (Hauck et al., 2023b). Models provide process-driven estimates of the CO_2 flux across the entire global ocean, drawing from the theory of ocean dynamics, biological and chemical processes (Hauck et al., 2020; Fennel et al., 2022). Despite the growing confidence in our mechanistic understanding of the ocean carbon cycle (Crisp et al., 2022), models are also subjected to uncertainty. This stems from uncertainties in model parametrizations, model spin-up and initial conditions, unresolved sub-gridscale processes and uncertainties in the atmospheric forcing (Hauck et al., 2020; Terhaar et al., 2024).

Data assimilation (DA) has been employed to address the emerging discrepancies between data products and models. So far, DA studies of the air-sea CO_2 flux have focused on specific regions (e.g. the Southern Ocean; Verdy and Mazloff, 2017), few years (e.g. 2009-2011; Brix et al., 2015) or the climatological mean state (e.g. Gerber et al., 2009); apart from a single multidecadal study covering the global ocean (Carroll et al., 2020). In each of these studies, an Adjoint or Green's Function DA approach is used to determine optimised boundary conditions, forcing terms and/or parameter values for the simulation. These studies capture well the assimilated pCO_2 observations, while obeying physical laws and biogeochemical (BGC) equations.

While previous studies indicate that the available BGC observations, when assimilated in isolation, are too sparse to constrain the modeled carbon cycle (Verdy and Mazloff, 2017), the assimilation of physical variables is expected to have a significant

https://doi.org/10.5194/egusphere-2024-1750
Preprint. Discussion started: 20 June 2024

indirect effect on the modeled CO_2 uptake because upwelling and subduction of DIC, as well as the physical transport of other biogeochemical tracers, will be affected (Doney et al., 2004). According to current knowledge, ocean physics is the dominant driver of interannual variability in the air-sea CO_2 flux (Doney et al., 2009; Keppler and Landschützer, 2019; Mayot et al., 2023; Liao et al., 2020). Furthermore, in GOBMs, well-constrained physics are particularly important to capture the ocean storage of anthropogenic carbon (C_{ant}), as the rate of anthropogenic CO_2 uptake depends ultimately on the modeled physical carbon transport from the air-sea interface across the mixed layer into the deep ocean in the form of dissolved inorganic carbon (DIC) (Davila et al., 2022). It was shown that assimilating ocean physics at the initial state of a model simulation has a stronger and more positive impact on the modeled carbon cycle than assimilating the BGC initial state (Fransner et al., 2020). Therefore the question arises which processes are most important when altered physics change CO_2 fluxes in DA approaches. We here use ensemble-based data assimilation of ocean physics into a global ocean biogeochemistry model to improve the modeled air-sea CO_2 flux for the years 2010-2020. For assimilation we use an ensemble Kalman filter variant (Nerger et al., 2012). With this approach, we describe the impact of continuously assimilating ocean-physics for eleven years on the model's air-sea CO_2 flux. Here, we identify the mechanisms of how physics DA affects the modeled air-sea CO_2 flux, differentiating between the thermally, DIC- and alkalinity induced components and changes in mixing, and lateral and vertical transport.

An accurate representation of ocean physics is a prerequisite, but not necessarily sufficient for a realistic simulation of the CO_2 flux. Coupled ecosystem models are adapted to the associated physics model with its strengths and weaknesses through carefully selected parameter values. Furthermore, the natural carbon cycle in models is tuned to an equilibrium for the physical model state at pre-industrial conditions without DA, and it was shown that the modeled carbon cycle may react very sensitive to deviations from this physical state, leading to biases in the carbon cycle through data assimilation (Spring et al., 2021).The question therefore arises as to what extent an ecosystem model coupled to a data-assimilated physical model also represents a more realistic biogeochemistry. We will present cases where physics data-assimilation leads to worse and better agreement with BGC observations. We focus, firstly, on the global air-sea CO2 flux. Secondly, we investigate the Southern Ocean given the relevant impact of DA in Southern Ocean winter. Thirdly, we present regions in the North Atlantic given observational coverage and relevant local processes there.

2 Methods

2.1 Model FESOM-REcoM

The oceanic model component, FESOM2.1, computes the advection, diffusion, and mixing of passive biogeochemical tracers. The model is based on hydrostatic primitive equations under the Boussinesq approximation and utilizes a finite-volume discretization approach with surface triangles projected vertically to form prisms. Salinity (S), temperature (T), and biogeochemical (BGC) tracers are located at the vertices of triangles (nodes), while the horizontal velocities are centered at the triangles (elements). The model allows for a variable mesh resolution and incorporates parametrizations for diffusion and eddy-stirring along isoneutral surfaces, for which parametrized mixing is scaled by mesh resolution (Danilov et al., 2017). Vertical mixing is parametrized through the KPP scheme and the mixing depth is specified through a boundary layer, with an

https://doi.org/10.5194/egusphere-2024-1750
Preprint. Discussion started: 20 June 2024

additional vertical mixing scheme used in the Southern Ocean. The surface salinity is restored towards climatology and scaled by a fictional flux at the ocean surface of 0.1m/day. A detailed description of FESOM2.1 is provided by Danilov et al. (2017) and a model assessment by Scholz et al. (2019, 2022).

The ocean biogeochemistry component, the Regulated Ecosystem Model version 3 (REcoM3), describes processes in the ocean carbon cycle and represents oceanic carbon in the form of dissolved inorganic carbon (DIC), dissolved organic carbon (DOC), plankton and detritus (Gürses et al., 2023). REcoM3 contains 28 BGC tracers (listed in Appendix Table A1). There are two phytoplankton groups: diatoms and small phytoplankton with implicit representation of calcifiers; two zooplankton groups: mixed and polar macro zooplankton (Karakuş et al., 2021); and two classes of detritus: fast and slow-sinking. REcoM3 includes variable intracellular stoichiometry with ratios of C:N:Chl:$CaCO_3$ for the small phytoplankton and C:N:Chl:Si for diatoms, which is propagated to zooplankton and detritus (Schartau et al., 2007; Hohn, 2008). The publicly available Routines To Model The Ocean Carbonate System (mocsy2.0) (Orr and Epitalon, 2015) are used to compute pCO_2 and air-sea CO_2 flux, employing the gas-exchange parameterization of Wanninkhof (2014). Alkalinity is restored by a fictional surface flux of 10m/yr. The current model version FESOM2.1–REcoM3 was assessed by Gürses et al. (2023) and previous versions were evaluated and applied in global and regional studies of the ocean carbon cycle and planktonic ecosystems (Hauck et al., 2013; Schourup-Kristensen et al., 2014; Hauck et al., 2020; Karakuş et al., 2021).

2.2 Data Assimilation

2.2.1 Assimilation method and implementation

For the assimilation, we use the Localized Error Subspace Transform Kalman Filter (LESTKF, Nerger et al., 2012). The LESTKF incorporates new observations as they emerge by updating the previous estimate of the state. The model state and error covariance are represented by an ensemble simulation. A review of the LESTKF and other filters frequently used in geophysics can be found in Vetra-Carvalho et al. (2018). The assimilation is implemented using the Parallel Data Assimilation Framework (PDAF2.1), a software environment for data assimilation. PDAF is an open source project and provides fully implemented DA algorithms (Nerger et al., 2020, pdaf.awi.de). The current implementation builds on the works of Mu et al. (2022) who used DA of ocean temperature and salinity for sea-ice forecasts with FESOM2.0 coupled to an atmospheric model, and Tang et al. (2020) who studied the dynamic impact of oceanic DA into FESOM1.4 onto a coupled atmospheric component.

With localization of the LESTKF, observations are weighted by distance, thereby avoiding the model being influenced by observations at distant locations through spurious correlations. We use a localization radius of 200 km and choose a 5th-order polynomial weighting function that mimics a Gaussian function (Gaspari and Cohn, 1999). We apply daily analysis steps at 0 UTC model time, assimilating all available observations for the day. The DA process only directly updates the physical model variables temperature, salinity, horizontal velocities and sea surface height. After each assimilation step, corrections are applied to the analysis state to ensure the consistency of model physics: Salinity is set to a minimum value of zero and temperature to a minimum value of $-2\,^{\circ}\mathrm{C}$, if necessary. The sea surface height (SSH) update is limited to two standard deviations of the ensemble. The analysis step is followed by an ensemble forecast of 1 day.

https://doi.org/10.5194/egusphere-2024-1750
Preprint. Discussion started: 20 June 2024

The ensemble size is 40, a compromise to balance computational resources while ensuring a sufficiently large ensemble with enough variability even in the deep ocean. The ensemble is generated through an initial perturbation of sea surface height, horizontal and vertical velocities, temperature, salinity and sea-ice concentration generated from a 1-year model run as described by Tang et al. (2020). To maintain ensemble spread, we apply a perturbed atmospheric forcing with an autoregressive perturbation $(\mathrm{perturb_n})$ at every model time step (n), with:

$$\mathrm{perturb_{n+1}} = (1 - \mathrm{arc}) * \mathrm{perturb_n} + \mathrm{arc} * s * (N_{\mathrm{ens}} - 1) * \mathrm{rand}$$

where rand is a stochastic element that is based on a covariance matrix derived from a 72-days-long period of atmospheric forcing; the autoregression coefficient (arc) is the inverse number of model steps per day; and s is a scaling factor for each perturbed atmospheric forcing field. For specific humidity, downwelling longwave radiation and air temperature $s = 10$ is used. The perturbation of winds is set to the smaller value $s = 2$ because the air-sea CO_2 flux in the model is particularly sensitive to perturbations of the wind fields. Because the ensemble spread still decays at each analysis step, an inflation of the ensemble is applied in each analysis step by applying a forgetting factor ρ (see e.g. Nerger et al., 2005). This inflation uses a time-varying forgetting factor between $\rho = 0.95$ and $\rho = 1$, where 1 means no inflation and smaller values mean larger inflation. The strongest inflation ($\rho = 0.95$) is applied during the first two weeks of the DA process. During the following 75 days ρ is increased to 0.99 and from thereon stays between 0.99 and 1.0 depending on a temperature threshold for the standard deviation of the ensemble spread.

2.2.2 Assimilated observations

We assimilate sea surface temperature (SST), sea surface salinity (SSS) and profiles of temperature (T) and salinity (S). The assimilated SST observations stem from the Operational Sea Surface Temperature and Ice Analysis (OSTIA) data set (CMEMS Marine Data Store; Good et al., 2020; Donlon et al., 2012; Stark et al., 2007). OSTIA provides daily gap-free maps of SST at a horizontal resolution of $0.05^\circ \times 0.05^\circ$, compiled from in-situ and satellite data from infrared and microwave radiometers. The OSTIA observations were averaged to the FESOM2.1 model grid because their spatial resolution is higher than the nominal resolution of the model grid. We prescribe an observation error standard deviation of $0.8\,^\circ\mathrm{C}$ for the DA (Nerger et al., 2020). Observations are excluded in the DA process, if the difference between the model and observation exceeds $2.4\,^\circ\mathrm{C}$ and at grid points with sea ice in the model, as in Tang et al. (2020) and Mu et al. (2022). This keeps the model stable despite large differences between model and observations at these sites, as water temperature and salinity develop differently under sea ice than under the influence of the atmosphere (Tang et al., 2020).

The assimilated SSS data is taken from the European Space Agency (ESA) Sea Surface Salinity Climate Change Initiative (CCI) (Boutin et al., 2021) v03.21 data set. ESA-CCI contains daily sampled SSS data at a spatial resolution of 50 km and a time resolution of 1 week. The ESA-CCI observations are averaged to the FESOM2.1 model grid. We prescribe a constant observation error standard deviation of 0.5 psu (Nerger et al., 2024). Like for the SST data, SSS observations are excluded at locations where sea ice is present in the model.

https://doi.org/10.5194/egusphere-2024-1750
Preprint. Discussion started: 20 June 2024

The assimilated temperature and salinity profiles are taken from the EN.4.2.2 data set (Good et al., 2013). The EN4 dataset contains quality-controlled profiles from various in-situ ocean profiling instruments. To assimilate the profile observations, the model values are computed as the average of the grid points of the triangle enclosing the observation because the number of observations is fewer than model grid points. The observation error standard deviation is set to $0.8\,^{\circ}\mathrm{C}$ for temperature and to 0.5 psu for salinity, as in Tang et al. (2020).

2.3 Simulation set-up

The model setup for both simulations closely follows (Gürses et al., 2023). The model mesh is irregular and has a nominal resolution of 1 degree, with enhanced resolution in the equatorial belt and north of $50\,^{\circ}\mathrm{N}$. It has 47 vertical layers with thickness ranging from 5 m at the surface to 250 m in the deep ocean, as described by Scholz et al. (2019). The model time step is 45 minutes. For atmospheric forcing, we use JRA55-do v.1.5.0, a reanalysis product tailored for driving ocean-sea-ice models (Tsujino et al., 2018). The atmospheric CO_2 mixing ratio (xCO_2) values were taken from the Global Carbon Budget (Joos and Spahni, 2008; Ballantyne et al., 2012; Friedlingstein et al., 2023). We use model restart fields from Gürses et al. (2023) where the model was spun-up by repeating the year-1961 JRA forcing for 189 years with preindustrial atmospheric CO_2 conditions, followed by a period from 1800 to 1957 with increasing atmospheric CO_2. Subsequently, simulations were continued with historical JRA forcing from 1958 to 2009. During the assimilation window (2010-2020), we conduct two ensemble simulations to study the impact of data assimilation (DA) covering the period of the years 2010 to 2020: one without DA (referred to as FREE) and another identical setup applying DA (referred to as ASML).

2.4 Data analysis

To assess the model results we focus on the ensemble mean. We present CO_2 flux estimates for the period 2010-2020, that are compared to the 'Regional Carbon Cycle Assessment and Processes 2' (RECCAP2) CO_2 flux estimates (DeVries et al., 2023). For the comparison of the global air-sea CO_2 flux in our simulations with the RECCAP2 CO_2 flux estimates, the river flux adjustment (Friedlingstein et al., 2023; Regnier et al., 2022) is applied to the pCO_2 products. Thus, we quantify the anthropogenic perturbation of the ocean carbon sink without rivers (as $\mathrm{S_{OCEAN}}$ in the Global Carbon Budget Friedlingstein et al., 2023; Hauck et al., 2020), and not the contemporary net air-sea CO_2 flux (as in RECCAP2).

To study the effect of DA on the CO_2 flux, we define regions where the effect is pronounced and where different mechanisms are active. In the Southern Ocean, we use the biomes defined by Fay and McKinley (2014). These are, from North to South, the Subtropical Seasonally Stratified Biome (STSS), the Subpolar Seasonally Stratified Biome (SPSS) and the Sea-Ice Biome (ICE) (see Fig. 5). Within the STSS, we differentiate between the area where the assimilation leads to a more positive air-sea CO_2 flux, referred to as STSS+ and the area where the assimilation leads to a more negative air-sea flux, the STSS- (Fig. 5a and b). In the North Atlantic, we consider four coherent regions, defined by the time-mean difference of the air-sea CO_2 fluxes in ASML and FREE ($\Delta F_{\mathrm{CO_2}}$, Fig. 6a and b). The Central STSS and Western STSS are located in the central North Atlantic STSS biome and are confined by $\Delta F_{\mathrm{CO_2}} < -1\,\mathrm{mmol\,C\,day^{-1}m^{-2}}$ and $\Delta F_{\mathrm{CO_2}} > 1\,\mathrm{mmol\,C\,day^{1}m^{-2}}$, respectively. The Newfoundland Basin and East Coast SPSS are part of the SPSS. The former is located east of Newfoundland and south

https://doi.org/10.5194/egusphere-2024-1750
Preprint. Discussion started: 20 June 2024

of Greenland, and is confined by $\Delta F_{CO_2} > 3\,\mathrm{mmol\,C\,day^{-1}m^{-2}}$; and the latter is located off the North American coast and confined by $\Delta F_{CO_2} < -1\,\mathrm{mmol\,C\,day^{-1}m^{-2}}$. The Central STSS and Western STSS lie on the warm side of the NAC, and the Newfoundland Basin and West Coast SPSS lie on the cold side of the NAC, which is evident from the modeled surface velocity field (Fig. A8).

Within these regions, we identify the time of the year when the DA affects air-sea CO_2 flux and calculate the difference of ASML and FREE for SST, SSS, surface velocities and transports, density, boundary layer depth, surface pCO_2, DIC, alkalinity and surface chlorophyll. In order to assess the drivers of dynamic DA effects on surface pCO_2, changes in pCO_2 are decomposed after the simulation into their contributions from changes in SST (SST), surface DIC (DIC) and alkalinity (Alk) following the linear approximations of Sarmiento and Gruber (2006) and Takahashi et al. (1993):

$$\Delta \mathrm{pCO_{2,DIC}} = \frac{\mathrm{pCO_2}}{\mathrm{DIC}} * \gamma_{\mathrm{DIC}} * \Delta \mathrm{DIC} \tag{1}$$

$$\Delta \mathrm{pCO_{2,Alk}} = \frac{\mathrm{pCO_2}}{\mathrm{Alk}} * \gamma_{\mathrm{Alk}} * \Delta \mathrm{Alk} \tag{2}$$

$$\Delta \mathrm{pCO_{2,SST}} = \mathrm{pCO_2} * \exp(0.0423 * \Delta \mathrm{SST}) \tag{3}$$

with

$$\gamma_{\mathrm{DIC}} = \frac{3 * \mathrm{Alk} * \mathrm{DIC} - 2 * \mathrm{DIC}^2}{(2 * \mathrm{DIC} - \mathrm{Alk})(\mathrm{Alk} - \mathrm{DIC})} \tag{4}$$

$$\gamma_{\mathrm{Alk}} = \frac{-\mathrm{Alk}^2}{(2 * \mathrm{DIC} - \mathrm{Alk})(\mathrm{Alk} - \mathrm{DIC})} \tag{5}$$

Values for γ_{DIC} and γ_{Alk} are excluded above 18 and below -19, respectively. This affects parts of the Southern Ocean SPSS and ICE biome (see white areas in Fig. 7b and c).

To evaluate the impact of the DA on the modeled biogeochemistry, we compare model outputs with independent observational datasets of surface pCO_2, DIC, alkalinity and surface chlorophyll. For each observation type (OBS), we define the improvement as:

$$\mathrm{improvement_{OBS}} = |\mathrm{FREE} - \mathrm{OBS}| - |\mathrm{ASML} - \mathrm{OBS}| \tag{6}$$

To evaluate surface pCO_2, we use observations from the Surface Ocean CO_2 Atlas (SOCAT Version 2023, Bakker et al., 2023, 2016), which are provided as a monthly gridded and quality-controlled compilation.

https://doi.org/10.5194/egusphere-2024-1750
Preprint. Discussion started: 20 June 2024

To assess DIC and alkalinity, we compare the modeled surface fields to the GLODAPv2.2023 bottle data (Lauvset et al., 2024b). At depth, we compare the model output to the GLODAPv2 DIC and alkalinity climatology (Lauvset et al., 2016), which is based on observations from the period 1972-2013 and normalized to 2002.

To evaluate global surface chlorophyll, we use observations from ESA-CCI, which is a multi-sensor satellite ocean-color chlorophyll-a dataset with monthly global coverage (Sathyendranath et al., 2021). In addition, for the Southern Ocean, we use the mean of three satellite products (Johnson et al., 2013) that were processed with more suitable algorithms for southern high latitudes.

3 Effect of DA on ocean physics

Before we investigate the CO_2 flux, we first evaluate the effect of DA on the modeled physics. In particular, we compare the model output of both simulations with the assimilated observations to verify that the assimilation brings them into better agreement with the observations. Additionally, we compare the temperature and salinity with the partly-independent EN4-OA product (Good et al., 2013, updated to version 4.2.2). EN4-OA is an objective analysis ingesting the assimilated EN4 profile data, interpolated to global coverage on 42 depth levels. Furthermore, we compare the sea-ice concentration with remote sensing observations from OSI-SAF (EUMETSAT, 2022).

The assimilation improves the agreement with the assimilated SST observations. On a global average, the SST in FREE is $0.14\,^{\circ}\mathrm{C}$ colder than the observations, which is estimated to lead to a solubility-driven global air-sea flux difference of $-0.06\,\mathrm{Pg\,C\,yr^{-1}}$. FREE exhibits an extensive cold bias of SST in the tropics and subtropics in all ocean basins and a warm bias in the Southern Ocean south of $40\,^{\circ}\mathrm{S}$, visible in Fig. 1a; mean state of SST in Fig. A1). Additionally, FREE shows regional SST biases in particularly near strong currents or in eddy-rich regions, such as the North Atlantic Current (NAC), Kuroshio, and the Southern Subtropical Front. The assimilation reduces the SST south of $40\,^{\circ}\mathrm{S}$ and in the North Pacific, and increases the SST in the tropics and subtropics (see Fig. 1b). The effect of DA is an absolute change by $0.30\,^{\circ}\mathrm{C}$ on global average and is particularly strong in the Southern Ocean and in the North Atlantic. Through the assimilation, the model state becomes more similar to the observations globally, which is evident from the positive improvement in Fig. 1c. In total, the global mean absolute difference in SST is reduced from $0.59\,^{\circ}\mathrm{C}$ to $0.32\,^{\circ}\mathrm{C}$. The assimilation-induced change in SST is estimated to drive a direct solubility-driven effect on the global-air sea CO_2 flux of $-0.14\,\mathrm{Pg\,C\,yr^{-1}}$. Yet, this global attribution is subject to high uncertainty due to the non-linear dependency of pCO_2 on temperature, and because regionally large effects with opposite signs lead to uncertainty in the global mean.

The assimilation also improves the agreement with the assimilated SSS observations. FREE shows a global SSS bias (0.49 psu, Fig. 1d). The assimilation leads to a global surface freshening (Fig. 1e). There are only a few regions where SSS in FREE is fresher than the observations and where the DA consequently increases the salinity. One of these regions lies in the North Atlantic. The assimilation improves the model-observation agreement in 91% of the observed ocean area, particularly much in the North Atlantic Central STSS and in the Southern Ocean STSS (Fig. 1f). Albeit negative side effects of temperature

https://doi.org/10.5194/egusphere-2024-1750
Preprint. Discussion started: 20 June 2024

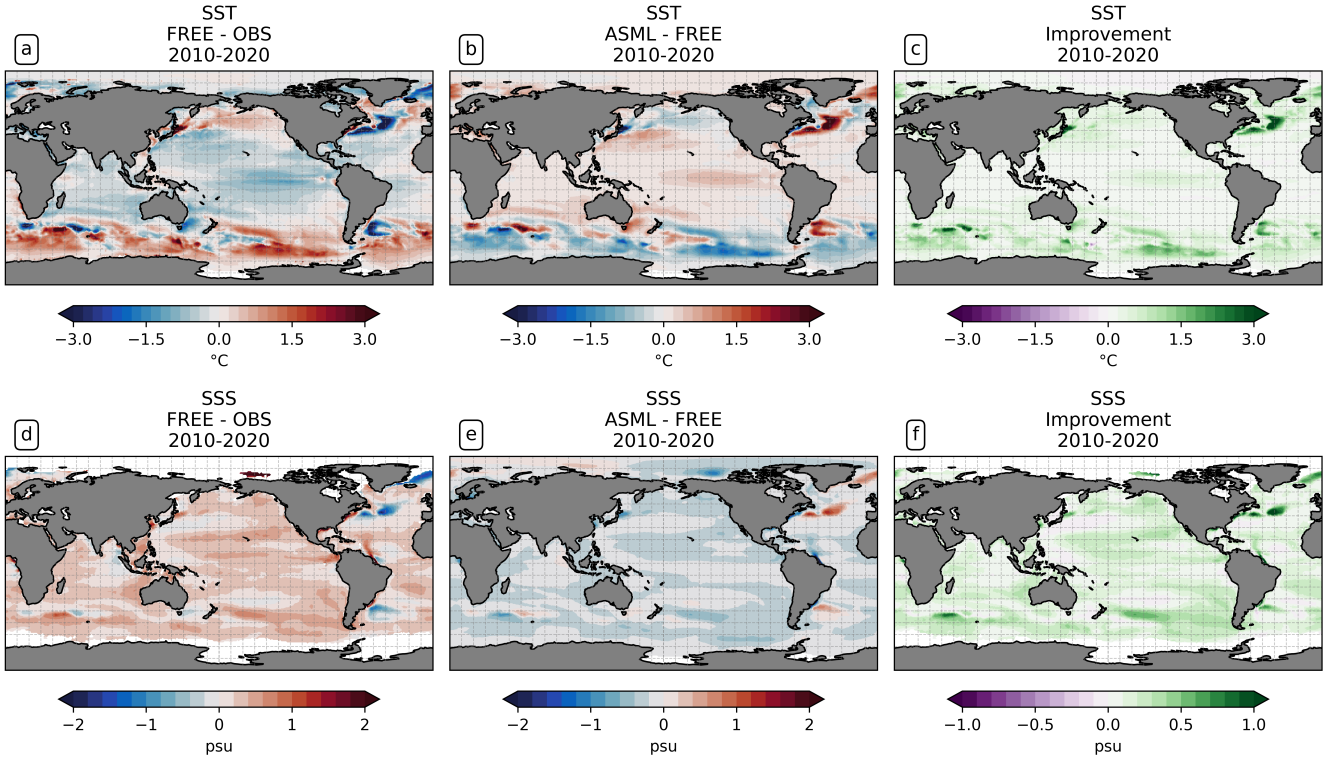

Figure 1. Effect of data assimilation on sea surface temperature (SST) and sea surface salinity (SSS). All panels show the mean over the period 2010-2020. (a) The model-observation difference in SST (FREE - OSTIA). (b) The difference ASML - FREE. (c) The improvement of monthly averaged model SST relative to OSTIA, where positive denotes that the assimilation brings the model closer to observations (Eq. (6)). (e - f) The same for SSS, computed with SSS from ESA-CCI.

assimilation on SSS in 9% of the observed area, the global mean absolute difference is reduced from 0.32 to 0.17 psu relative to the observations. The direct solubility-driven effect on the global air-sea CO_2 flux is estimated to be negligible.

The assimilation leads to a better agreement with subsurface temperature and salinity data from the non-assimilated EN4-OA product in the upper 1000 m. In the upper 100-200 m of the ocean, the model-observation difference in temperature follows the surface signal (compare Fig. 1a and Fig. 2a), and the difference is reduced by the assimilation (Fig. 2b and c). At intermediate depth (roughly 200-500 m), a subsurface warm bias exists in FREE in the southern hemisphere at mid-latitudes (Fig. 2; mean state in Fig. A2). This bias affects the South Pacific, South Atlantic and southern Indian Ocean (not shown). It might be connected to the model's surface warm bias in the formation region of Antarctic intermediate water (Fig. 1a). Further model-observation differences exist at greater depth than 500 m, where the model's subsurface temperature is colder than the observations at almost all latitudes, but warmer than the observations north of 60 °N. At most latitudes and depths, the effect of the assimilation is to reduce the model observation-differences. This can be seen from the difference of ASML and FREE, which has a reversed sign (compare Fig. 2a and Fig. 2b). Thereby, the improvement through DA is mostly positive (Fig. 2c).

https://doi.org/10.5194/egusphere-2024-1750
Preprint. Discussion started: 20 June 2024

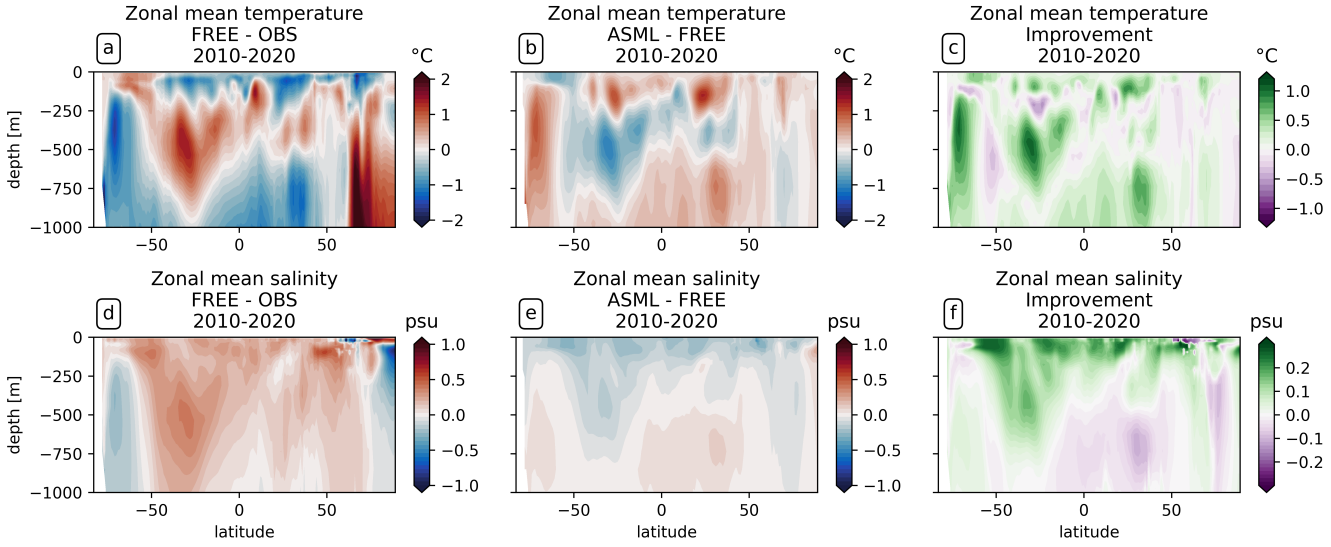

Figure 2. Effect of data assimilation on zonally averaged temperature and salinity in the upper 1000 m. All panels show the mean over the period 2010-2020. (a) The model-observation difference in temperature (FREE - EN4-OA). (b) The difference ASML - FREE. (c) The improvement of monthly averaged temperature relative to EN4-OA. (d - f) The same for salinity.

For the salinity, the model is more saline than the observations from the surface down to a depth of about 1000 m for most latitudes (Fig. 2d). This shows that the model-observation difference in this depth range follows the surface signal. The exceptions to this are at high latitudes below 200 m, where FREE is fresher than the observations. At all other latitudes, the assimilation acts towards a freshening, with the strongest effect near the surface (Fig. 2e). This improves the agreement with observations particularly near the surface (Fig. 2d). However, the improvement is smaller at depth and becomes even negative for some latitudes in greater depth. This might be due to the limited amount of assimilated in situ salinity profiles.

The effect of the assimilation on temperature and salinity is most pronounced in the upper 1000 m and, below that, mostly decreases with depth (not shown). After the second year of assimilation, the mean absolute difference between ASML and FREE stabilizes in the range $0.35 - 0.36\,^{\circ}\mathrm{C}$ for SST and $0.20 - 0.25\,\mathrm{psu}$ for SSS, while the difference of the 3D fields keeps increasing throughout the years 2010-2020.

Sea ice reacts dynamically to the changed ocean physical state. In the Southern Ocean, FREE is characterized by a lower sea-ice concentration compared to OSI-SAF observations. The maximum extent of sea-ice in September is smaller in FREE than OSI-SAF, which is demonstrated by the 15%-lines for FREE and OSI-SAF (Fig. 3a; mean state of sea-ice concentration in Fig. A3), and by the sea-ice concentration difference for the month September (Fig. 3b). Through DA, a higher Antarctic sea-ice concentration is obtained (see Fig. 3b). This improves the agreement with OSI-SAF (Fig. 3c). During all other seasons, the assimilation leads to a higher sea-ice concentration in the Antarctic, a larger sea-ice extent and a better agreement with OSI-SAF as well (only September is shown). In the Arctic, the differences between FREE, ASML and OSI-SAF are regionally different (not shown).

https://doi.org/10.5194/egusphere-2024-1750
Preprint. Discussion started: 20 June 2024

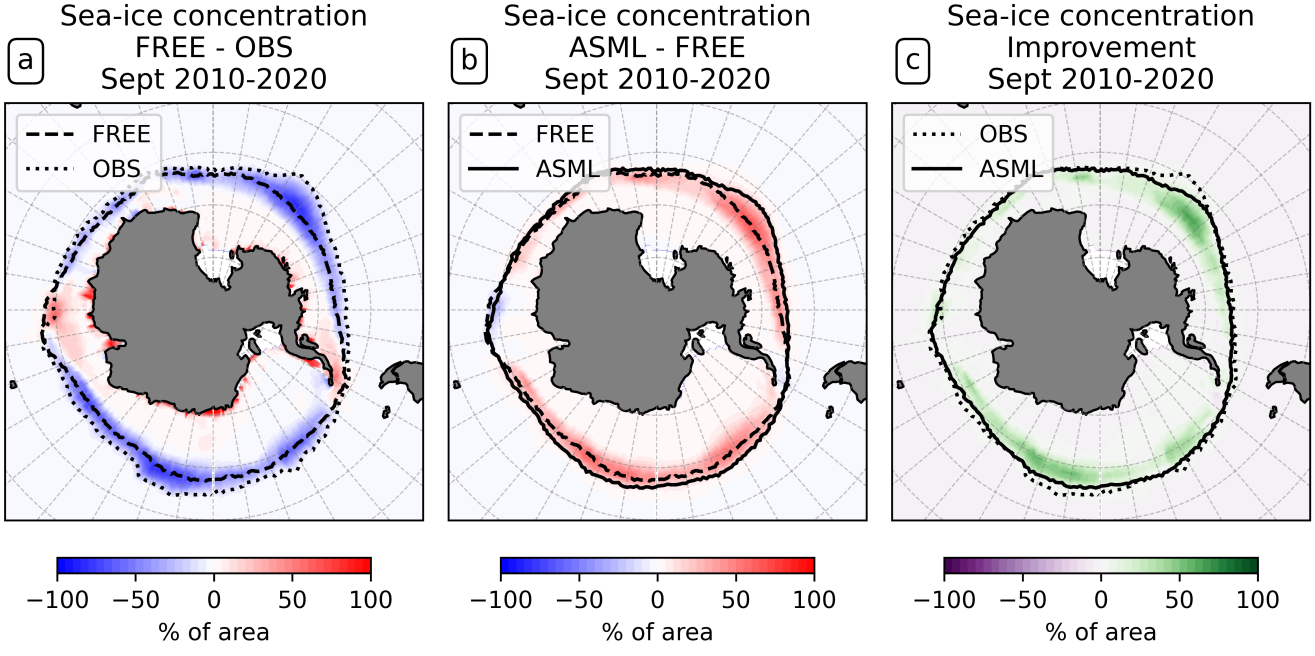

Figure 3. Effect of data assimilation on Antarctic sea-ice concentration in September. All panels show differences in the sea-ice concentration averaged for the month September over the period 2010-2020. The 15%-line for FREE, ASML and OSI-SAF observations is shown as a dashed, continuous or dotted line in panels a or b, respectively. (a) The difference between FREE and OSI-SAF observations. (b) The difference between ASML and FREE. (c) The improvement of September mean sea-ice concentration.

A common issue in data assimilation in GOBMs is erroneous equatorial upwelling, leading to unrealistically high biological productivity in the tropics (Park et al., 2018). In FESOM-REcoM, the biological productivity near the equator is stable in ASML. The meridional overturning, however, shows spurious structures, which may point to hidden assimilation artifacts on vertical velocities (see Appendix Text A1 for further discussion). The temperature and salinity fields at and near the surface in ASML are in good agreement with the observations. Thus, it can be assumed that the velocities in the upper part of the ocean are also well represented. Therefore, we are confident that the DA provides an improved physical state in the upper ocean, which serves as an improved basis to estimate the air-sea CO_2 flux, although the spurious effects on deep ocean circulation should be further addressed in future work.

4 Results

4.1 Global CO_2 flux

The ocean absorbs $2.78\,\mathrm{Pg\,C\,dec^{-1}}$ in ASML and $2.83\,\mathrm{Pg\,C\,dec^{-1}}$ in FREE during 2010-2020 (Fig. 4b), thus the assimilation decreases the global mean oceanic CO_2 uptake by $0.05\,\mathrm{Pg\,C\,dec^{-1}}$. The temporal evolution of the annual global CO_2 flux is

https://doi.org/10.5194/egusphere-2024-1750
Preprint. Discussion started: 20 June 2024

similar in ASML and FREE (Fig. 4a). The first assimilation year, 2010, stands out because it is one of the very few years during which the assimilation increases the oceanic CO_2 uptake. This slightly reduces the trend in CO_2 uptake 2010-2020 ($(-0.40 \pm 0.09)\,\mathrm{Pg\,C\,dec^{-1}}$ versus $(-0.38 \pm 0.11)\,\mathrm{Pg\,C\,dec^{-1}}$). The trend, thereby, remains within its confidence interval. Furthermore, the assimilation reduces the interannual variability of the global mean oceanic uptake slightly, demonstrated by a standard deviation of detrended annual means of $0.11\,\mathrm{Pg\,C\,dec^{-1}}$ in FREE and $0.08\,\mathrm{Pg\,C\,dec^{-1}}$ in ASML (not significantly different according to F-test).

The strongest time-mean air-sea CO_2 flux (negative: into the ocean) is found at mid and high latitudes (Fig. 4c). The large-scale pattern of the CO_2 flux is generally very similar in FREE and in ASML (FREE not shown). However, the effect of the assimilation on the CO_2 flux varies from region to region (Fig. 4d). The largest local changes, both towards stronger or weaker CO_2 fluxes, occur in the North Atlantic in the area of the NAC and in the coastal North Pacific. The most prominent large-scale effect though, is in the Southern Ocean. South of $50\,^{\circ}\mathrm{S}$, the area-integrated CO_2 uptake increases by $0.18\,\mathrm{Pg\,C\,dec^{-1}}$ through the assimilation (Fig. 4e and f). In contrast, the uptake decreases by $0.07\,\mathrm{Pg\,C\,dec^{-1}}$ between 40-$50\,^{\circ}\mathrm{S}$. With the exception of the Southern Ocean, CO_2 uptake decreases in all world oceans by a small amount (Fig. 4d and e).

4.2 Regional CO_2 fluxes and their drivers

The impact of the DA on the CO_2 flux is particularly large in the Southern Ocean, where we now inspect individual regions. In the northernmost biome of the Southern Ocean, the subtropical seasonally stratified biome (STSS, outlined in Fig. 5a), the mean oceanic CO_2 uptake is high (Fig. 5a). Here, the uptake is largest in austral winter and spring (June to November, Fig. 5c and d). In the more northern part of the STSS, which we call the STSS+, the CO_2 uptake is reduced through the assimilation, demonstrated by a positive flux difference between ASML and FREE in this area (Fig. 5b). The reduction is greatest in winter and spring, which is shown through a positive flux difference between ASML and FREE from July to October (Fig. 5g). In contrast, in the more southern part of the STSS, which we call the STSS-, the assimilation increases the oceanic CO_2 uptake (Fig. 5b). The increase of CO_2 uptake through DA is largest in summer and autumn (November to April, Fig. 5h).

Further south, in the subpolar seasonally stratified biome (SPSS), the ocean absorbs CO_2 all year-round (Fig. 5a). The oceanic uptake is increased through the assimilation, shown by a negative difference of ASML and FREE in Fig. 5b. The largest difference between ASML and FREE is seen in spring from September to October (Fig. 5i). Due to the seasonal effect of DA, the seasonal cycle of the CO_2 flux in the SPSS is altered. In ASML, the CO_2 uptake is weakest in February, gets stronger in autumn (MAM), stalls growing in winter (JJA) and resumes to get stronger in spring (SON), reaching peak uptake in November (Fig. 5e). In FREE, the CO_2 uptake is weakening in winter, is weakest in September and gets stronger afterwards, reaching peak uptake in December.

In the seasonally ice-covered biome (ICE) surrounding the Antarctic continent, the time-mean CO_2 flux is smaller than in the other biomes (Fig. 5a). In this region, the ocean absorbs CO_2 during summer and there is a smaller outgassing during winter (Fig. 5f), as the region is mostly ice-covered in winter (see sea-ice concentration in September in Fig. 3). In the northern part of the ICE biome, close to the SPSS, the effect of the assimilation is similar to the effect within the SPSS itself (Fig. 5b). Here, the assimilation acts to increase ocean CO_2 uptake or to weaken CO_2 outgassing during winter and spring (Fig. 5i and j).

https://doi.org/10.5194/egusphere-2024-1750
Preprint. Discussion started: 20 June 2024

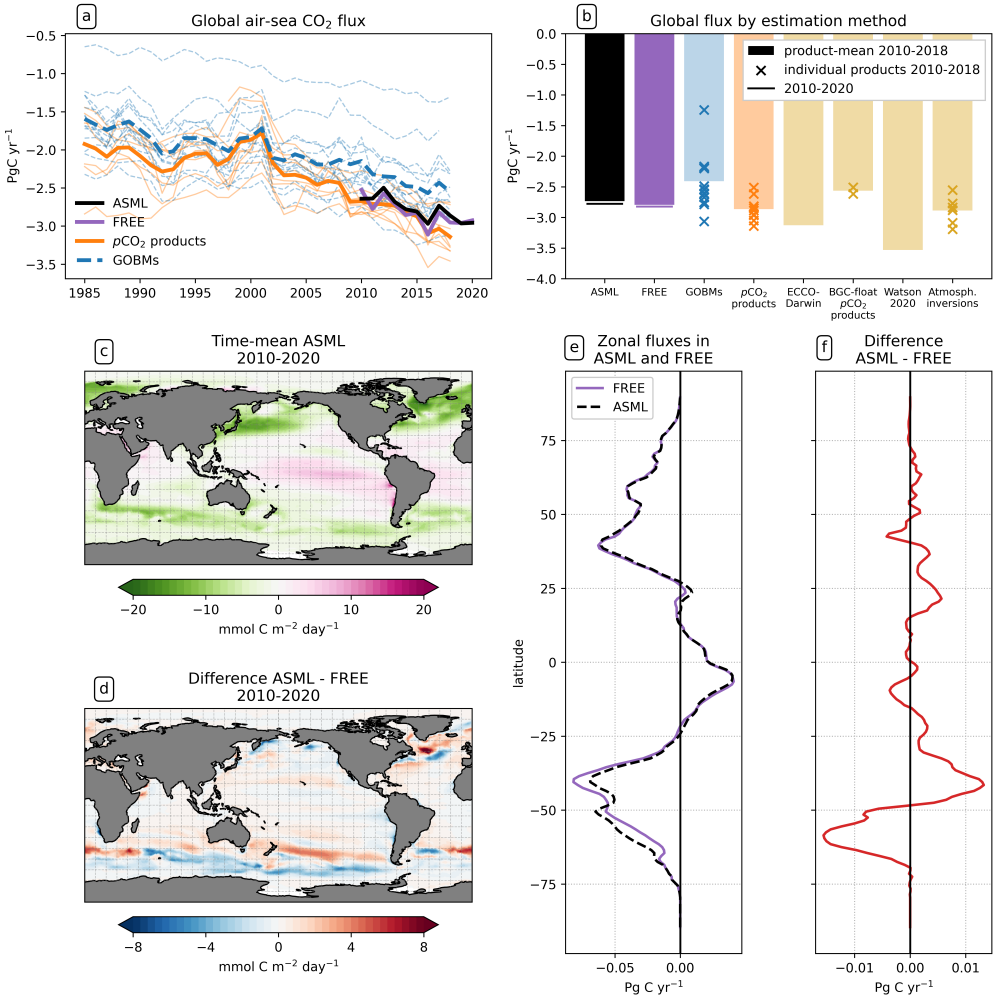

Figure 4. Effect of data assimilation on the air-sea CO_2 flux (negative: into the ocean). (a) Annual time-series of global flux in $\mathrm{Pg\,C\,dec^{-1}}$ in FESOM-REcoM-PDAF with ASML (black) and FREE (violet); and RECCAP estimates (DeVries et al., 2023) with pCO_2-products (orange) and GOBMs (blue) and their respective ensemble means (bold lines). Here, the river flux adjustment ($-0.65\,\mathrm{Pg\,C\,dec^{-1}}$) was applied to the pCO_2 products. (b) Time-mean global flux 2010-2018 in ASML (black), FREE (violet); and RECCAP estimates grouped by method (DeVries et al., 2023). Crosses represent individual estimates (e.g. individual GOBMs) and bars represent the ensemble mean (e.g. mean of twelve GOBMs). Here, the river flux term was applied to all estimates except the models following the Global Carbon Budget methodology (Friedlingstein et al., 2023). For FESOM-RECoM-PDAF, additionally the time-mean 2010-2020 is shown (horizontal lines). (c) Spatial distribution of CO_2 flux averaged over the period 2010-2020 in ASML. (d) Spatial distribution of CO_2 flux difference between ASML and FREE averaged over the period 2010-2020 (e) Zonal averages of CO_2 flux 2010-2020 in ASML and FREE, and their difference in (f).

https://doi.org/10.5194/egusphere-2024-1750
Preprint. Discussion started: 20 June 2024

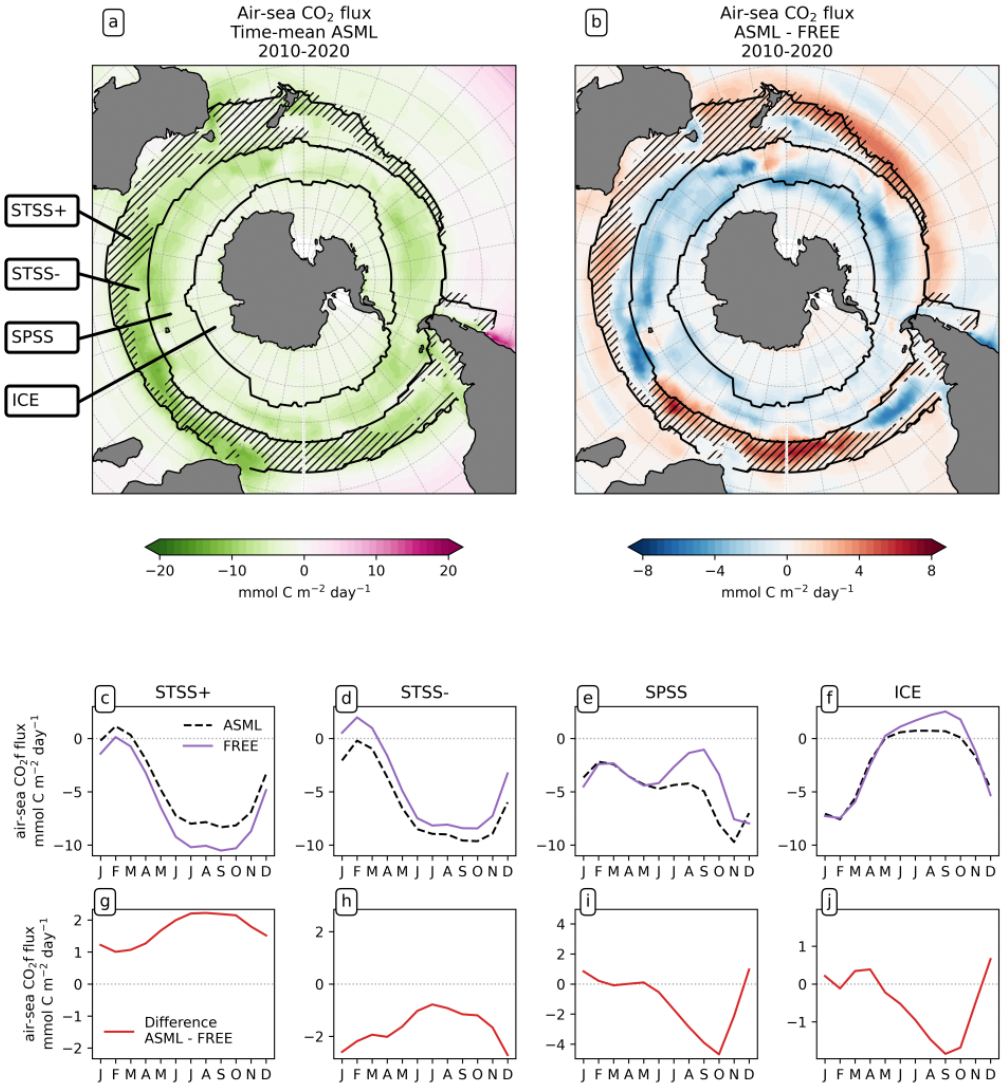

Figure 5. Effect of data assimilation on Southern Ocean CO_2 flux and its seasonality averaged over the period 2010-2020. Negative numbers indicate a flux into the ocean. (a) Map of mean CO_2 flux in ASML. (b) Map of difference between CO_2 flux in ASML and FREE. (c - f) Seasonal cycle of air-sea CO_2 flux by region. (g - j) Seasonal difference in air-sea CO_2 flux between ASML and FREE by region. Note the different scales.

Thereby, interestingly, the assimilation hinders outgassing of CO_2 from May to November in ASML in the ICE biome (Fig. 5f; comparison of winter outgassing with other estimates in Fig. A4). In the southern part of the ICE biome, near the Antarctic continent, the effect of the DA on the CO_2 flux is small.

In the North Atlantic, the assimilation has noticeable effects on the CO_2 flux in the area of the NAC. In this region, the ocean absorbs CO_2 in the annual average (Fig. 6a). However, the ocean releases some CO_2 during summer, while the sea surface

https://doi.org/10.5194/egusphere-2024-1750
Preprint. Discussion started: 20 June 2024

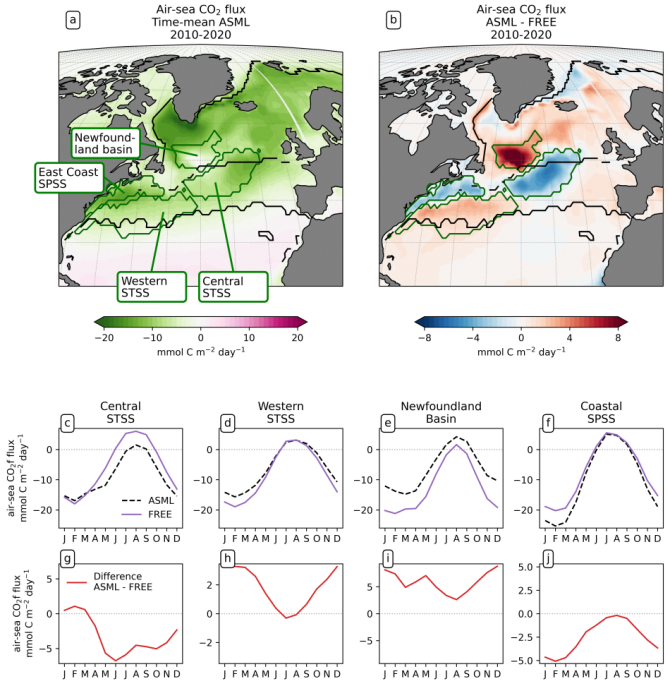

Figure 6. Effect of data assimilation on North Atlantic CO_2 flux and its seasonality averaged over the period 2010-2020. Negative numbers indicate a flux into the ocean. (a) Map of mean CO_2flux in ASML. (b) Map of difference betweenCO_2flux in ASML and FREE. (c - f) Seasonal cycle of air-seaCO_2flux by region. (g - j) Seasonal difference in air-seaCO_2flux between ASML and FREE by region. Note different scales.

warms (Fig. 6c-f). In the Central STSS, the effect of the DA is to prevent outgassing during summer (Fig. 6c and g). In the Western STSS and in the Newfoundland Basin, the ocean CO_2 uptake is decreased during winter (Fig. 6d,e,h and j). In the East Coast SPSS, the ocean CO_2 uptake is increased (Fig. 6f and j). The regionally different dynamics of the effects of the assimilation that drive these differences in the air-sea CO_2 flux in the North Atlantic and Southern Ocean, will be investigated next.

In the Southern Ocean, the reduced CO_2 uptake and increased pCO_2 in the STSS+ region is driven by increased surface DIC and lowered alkalinity (Fig. 7b and c, hatched area). These, as well as the colder SST and fresher SSS in the STSS+ region (Fig. 1b and e) are indications for a year-round stronger influence of subantarctic waters. This is evident as in the subantarctic, surface DIC is higher and surface alkalinity is lower than in the subtropical Southern Ocean (Fig. A5c and d), and, furthermore, the subantarctic is characterized by cold temperatures and low salinity (Fig. A5 a and b). In addition, reduced net primary production (NPP) in spring contributes to higher DIC in the STSS+ region in ASML (not shown). In contrast, the increased CO_2 uptake and reduced pCO_2 in the STSS- is driven by lower surface DIC and by increased alkalinity (Fig. 7b and c, non-hatched area). These, together with higher SST in ASML than FREE in the STSS- regions (Fig. 1b), indicate a higher presence of subtropical waters (see characteristics of subtropical waters in Fig. A5). Moreover, higher NPP contributes to lower

https://doi.org/10.5194/egusphere-2024-1750
Preprint. Discussion started: 20 June 2024

DIC in the STSS- region in ASML (not shown). The seasonality of the effect of DA on the air-sea CO_2 flux (Fig. 5c-d,g-h) is determined by seasonal temperature differences between ASML and FREE (Fig. 7d-g). In the STSS+ region, SST is slightly reduced during summer (Fig. 7f). This lowers pCO_2 in the STSS+ region (Fig. 7a), counteracts the effects of DIC and alkalinity on pCO_2 and thus dampens the overall effect on the air-sea CO_2 flux during summer. In contrast, in the STSS- region, the SST is higher in ASML than FREE during winter (Fig. 7e and g). This increases pCO_2 in the STSS- region (Fig. 7a), counteracting the effects of lower DIC and higher alkalinity on pCO_2 and dampening the overall effect during winter. In summary, the contrasting effects in the STSS are probably generated by a horizontal redistribution of water masses within the STSS biome. In the center of the STSS, the Subantarctic Front is located, which is associated with the Antarctic Circumpolar Current (ACC) and characterized by a strong gradient in SST, SSS and various other tracers (Chapman et al., 2020). Because SST and SSS are directly influenced and improved by the assimilation, the position of this front is also expected to change as a result of the assimilation, leading to a horizontal relocation of waters separated by the front. In addition, differences in the horizontal transport of DIC and alkalinity by the ACC (transport not shown), and differences in the velocities between ASML and FREE (Fig. A6), indicate a horizontal redistribution with zonal and meridional components.

In the SPSS, the increased CO_2 uptake and lower surface pCO_2 during winter and spring is driven by a combination of lower DIC and colder temperatures (Fig. 7a and b), which outweigh the opposite effect of a decrease in alkalinity on pCO_2 (Fig. 7c). Surface DIC is generally high due to upwelling of carbon-rich deep water (Hauck et al., 2023a). The reason for lower surface DIC in ASML is likely that the upward transport of DIC is reduced through a more stable stratification, which is shown by a reduced density in the upper 300 m and an increased density below that (Fig. 7h). Thereby, the densities in the SPSS agree better with densities calculated from EN4-OA. The more stable stratification reduces the depth of the boundary layer in winter and spring (not shown). Vertical mixing within the boundary layer affects the vertical profile of DIC, towards lower DIC in ASML above 100 m and higher DIC below (Fig. 7i). The vertical profile of DIC in ASML is closer to GLODAP DIC observations, albeit some differences to GLODAP still exist. Besides the fact that the differences in stratification and boundary layer depth affect the vertical DIC profile, they also imply less available surface nutrients in ASML. Probably due to that, in the SPSS, ASML features lower NPP, lower chlorophyll concentrations and a lower phytoplankton biomass (not shown).

In the Northern part of the ICE biome near the SPSS, the reduced outgassing and decreased pCO_2 during winter and spring is driven by similar processes as within the SPSS. Again, lower surface DIC and colder temperatures (Fig. 7a and b) outweigh the opposite effect of a decrease in alkalinity on pCO_2 (Fig. 7c). As in the SPSS, the reason for the decrease in pCO_2, is, firstly, a more stable stratification through surface freshening, which reduces DIC above 100 m depth and increases DIC below (not shown). Secondly, as the surface temperature is lower in ASML (Fig. 1b), the winter sea-ice concentration is higher (Fig. 3b), which prevents winter outgassing of CO_2.

In summary, in the Southern Ocean, the main effects of the DA on the CO_2 flux are, firstly, an increase of the uptake in the SPSS caused by a more stable stratification and thus less upward transport of naturally carbon-rich water through mixing and secondly, an overall decrease of uptake in the STSS as a consequence from a horizontal redistribution of water masses within the STSS.

https://doi.org/10.5194/egusphere-2024-1750
Preprint. Discussion started: 20 June 2024

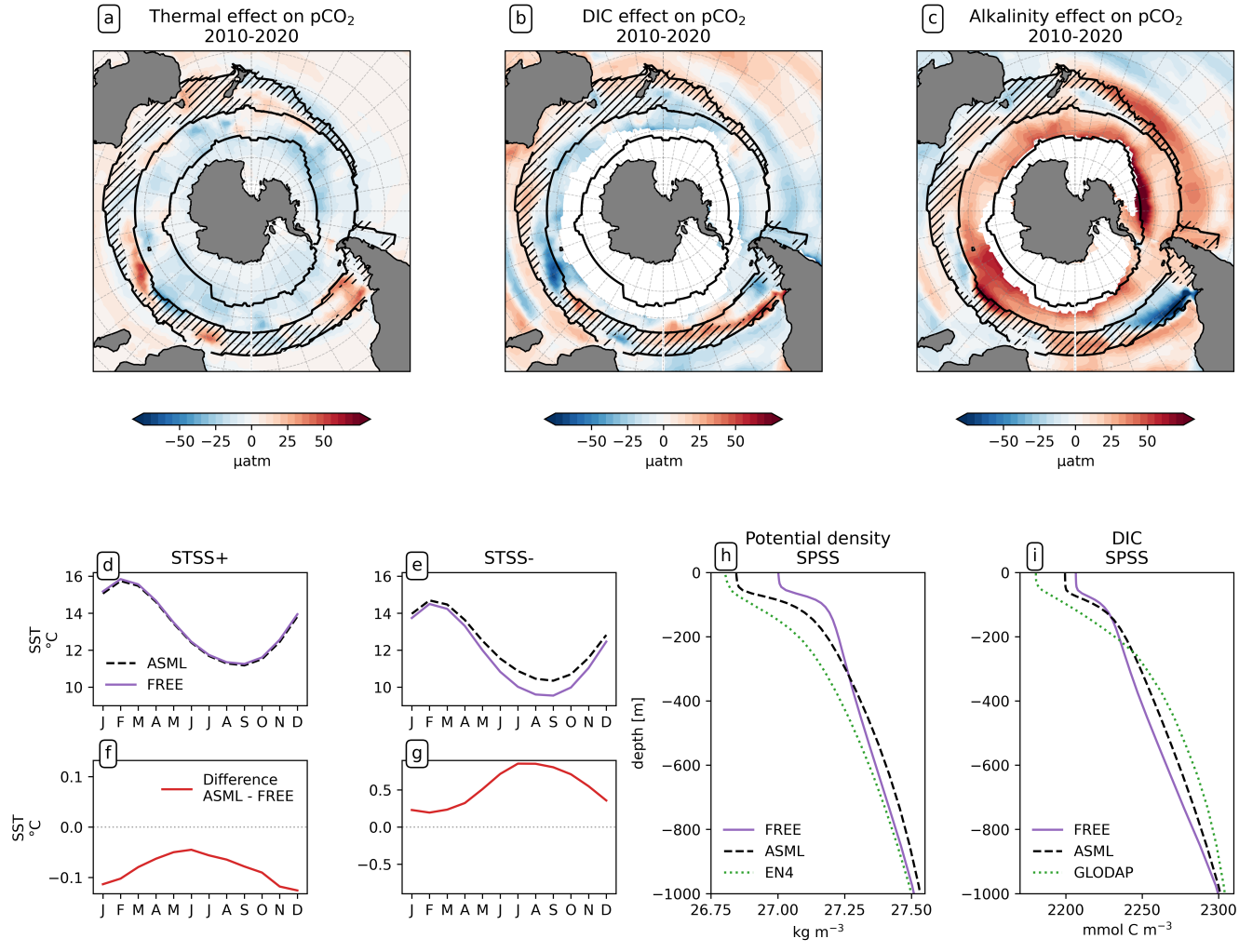

Figure 7. Drivers of the effects of data assimilation on air-sea CO_2 fluxes in the Southern Ocean. Panels a, b and c show the effects of SST, DIC and alkalinity differences between the ASML and FREE simulations on surface pCO_2, where positive denotes an increase in pCO_2. Hatching inside the STSS indicates where net pCO_2 is increased through the assimilation (STSS+). (d and e) Seasonal cycle of SST averaged over the regions STSS+ and STSS- for the ASML and the FREE, and (f and g) the difference between ASML and FREE for each region. (h) Potential density profiles for the SPSS in the Southern Ocean, with FREE (violet line) and ASML (dashed black line) based on daily T and S, and with EN4-OA (dotted green line) based on monthly T and S. (i) DIC profiles for the SPSS in the Southern Ocean, showing FREE (violet line), ASML (dashed black line) from 2010-2020 and climatological DIC from GLODAP.

https://doi.org/10.5194/egusphere-2024-1750
Preprint. Discussion started: 20 June 2024

In the North Atlantic, the effects of the DA on the CO_2 flux are locally large, but there are differences to the Southern Ocean. In the Central STSS, the effect of the DA is towards increased uptake of CO_2 during boreal summer and autumn in ASML (Fig. 6g). This prevents summer outgassing, which occurs from June to October in FREE (Fig. 6c). The reason for the higher uptake and decreased surface pCO_2 is higher alkalinity in ASML (Fig. 8b). In this region, the alkalinity effect, which reduces pCO_2, outweighs the opposing effects of DIC and SST on pCO_2 (Fig. 8a and c). A higher alkalinity could point to the presence of waters of subtropical origin (Fig. A7d), transported northward with the NAC (Völker et al., 2002). Other fingerprints of waters advected by the NAC are a warm SST particularly in winter, a higher salinity and higher DIC than that of North Atlantic subpolar waters (Fig. A7a-c, Völker et al., 2002). The assimilation causes a change in these properties, towards a higher SST, higher salinity and higher DIC in the Central STSS (Fig. A7). Simultaneously, ASML represents higher NPP, biological carbon export at 200 m, surface chlorophyll and column integrated phytoplankton biomass in spring, which is shown by the example of surface chlorophyll difference between ASML and FREE in Fig. 8e. This is facilitated by more available nutrients through winter mixing in the surface boundary layer, which is deeper in ASML (Fig. 8d). In combination, the higher biological export of carbon and the higher alkalinity in ASML result in lowered surface pCO_2 and higher oceanic uptake.

In the Western STSS, the DA reduces the CO_2 uptake and increases pCO_2 mainly during winter, as a direct effect of increased SST (Fig. 8a). In this region, the thermal effect of DA, which increases pCO_2, is dominant over the combined effect of DIC and alkalinity. The latter have effects comparable in magnitude to SST, but mostly cancel each other out (Fig. 8b-c). The effect of DA on surface properties (SST, SSS, DIC and alkalinity) in the Western STSS is similar to the effect in the Central STSS, which indicates a higher influence of subtropical waters in both regions.

In the Newfoundland Basin, the dominant effect of DA is a reduction of the CO_2 uptake and an increase of pCO_2 mainly during winter, as a direct effect of increased SST (Fig. 8a). In addition, ASML also features shallower winter mixing inside the boundary layer (Fig. 8d) and a more stable stratification due to lower density at the surface than FREE (Fig. 8f). Consequently, DIC and alkalinity in the upper 100 m are slightly reduced. Neverless, some differences to GLODAP-DIC observations remain (DIC in Fig. 8g). However, the thermal effect of DA, which increases pCO_2, is dominant over the combined effect of DIC and alkalinity on pCO_2 (Fig. 8b and c), as the latter cancel each other out. Furthermore, surface nutrients, NPP, export production, biomass and surface chlorophyll are reduced (surface chlorophyll in Fig. 8e), probably due to shallower mixing. In the Western Boundary STSS, the increased CO_2 uptake and reduced pCO_2 in ASML during winter and spring is facilitated by colder SST (Fig. 8a). This might be due to subpolar water masses penetrating further south along the coast in ASML because the location where the current separates from the coast is further south in ASML (Fig. A8). In summary, DA affects the CO_2 flux in the North Atlantic mainly through horizontal and vertical redistribution of DIC and alkalinity, and through changes in SST. However, which of these effects is dominant varies from region to region.

4.3 Comparison with biogeochemical observations

To evaluate the modeled air-sea CO_2 flux based on observations, surface pCO_2 is the most informative variable, as it is closely related to the air-sea CO_2 flux. Effects of the DA on the modeled ecosystem and associated carbon fluxes, as well as thermal and dynamical effects that affect the CO_2 flux, are all included in pCO_2. The global mean of absolute monthly model-observation

https://doi.org/10.5194/egusphere-2024-1750
Preprint. Discussion started: 20 June 2024

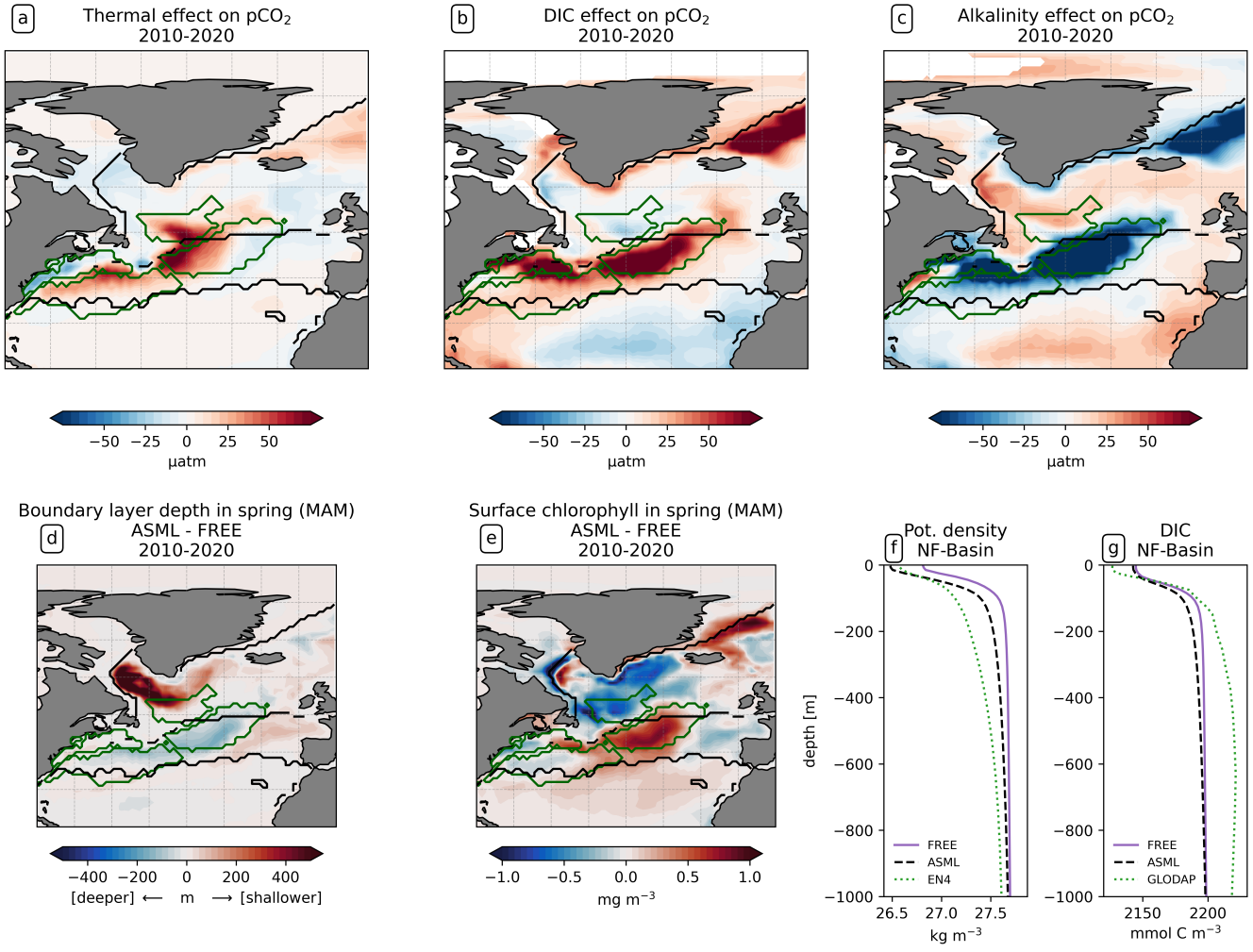

Figure 8. Drivers of the effects of data assimilation on air-sea CO_2 flux in the North Atlantic. Panels a, b and c show the effects of SST, surface DIC and alkalinity differences between ASML and FREE on surface pCO_2. (d) Difference of boundary layer depth (ASML - FREE) for spring (MAM) 2010-2020, where positive denotes a shallower boundary layer in the ASML. (e) Difference of surface chlorophyll (ASML-FREE) for spring (MAM) 2010-2020. (f) Potential density profiles for the Newfoundland Basin region, with FREE (violet line) and ASML (dashed black line) based on daily T and S, and with EN4-OA (dotted green line) based on monthly T and S. (g) DIC profiles for the Newfoundland Basin region, showing FREE (violet line), ASML (dashed black line) from 2010-2020 and climatological DIC from GLODAP.

https://doi.org/10.5194/egusphere-2024-1750
Preprint. Discussion started: 20 June 2024

differences to the available SOCAT pCO_2 observations is $27.26\,\mu atm$ for FREE. For ASML, the difference is slightly larger with $27.60\,\mu atm$. On global average, pCO_2 is higher than in SOCAT by $3.70\,\mu atm$ in FREE and $4.59\,\mu atm$ in ASML, as regions with positive and negative differences to SOCAT compensate (Fig. 9a). The assimilation changes pCO_2 by a mean absolute value of $8.08\,\mu atm$, which is $\pm 27\%$ of the mean absolute model-observation difference. A linear offline estimation demonstrates that this change in pCO_2 would lead to an absolute change in the air-sea CO_2 flux by $1.06\,mmol\,C\,m^{-2}\,day^{-1}$ on average.

Overall, FREE and ASML show very similar regional pCO_2 differences compared to SOCAT (difference of FREE and SOCAT in (Fig. 9a); difference of ASML and SOCAT not shown). In the subtropical and tropical Atlantic and the subtropical Pacific, FREE and ASML have higher pCO_2 than SOCAT, while in the equatorial Pacific, the pCO_2 is lower. At high latitudes, FREE and ASML represent mostly lower pCO_2 than SOCAT.

In the Southern Ocean, the simulations represent lower pCO_2 than SOCAT in the SPSS and ICE biomes in the annual mean (Fig. 9c), which is dominated by summer differences to SOCAT (not shown) when most observations are available. Through the assimilation, pCO_2 is increased in summer and reduced in winter (not shown), leading to an overall better agreement with SOCAT (Fig. 9e). In contrast, in the STSS, FREE and ASML represent higher pCO_2 than SOCAT, and through the assimilation, the agreement with SOCAT decreases.

In the North Atlantic, the simulations and SOCAT show a similar large-scale pattern, namely that pCO_2 is higher in the subtropics (ASML: around $400\,\mu atm$) than in the subpolar regions (ASML: around $280\,\mu atm$). Yet, this latitudinal difference of pCO_2 is stronger in the simulations compared to SOCAT, meaning that in the subtropics, pCO_2 in the simulations is higher than in SOCAT (Fig. 9d), while it is lower in the subpolar regions. Furthermore, in both simulations there is a pronounced pCO_2 surface gradient in the NAC and Subpolar Gyre region, whose position is changed by the assimilation, and which appears to be further northward in SOCAT. Thereby, the assimilation overall leads to a better agreement with SOCAT, in particular through a decrease of pCO_2 in the Central STSS, where the average difference is reduced from $26\,\mu atm$ (FREE - SOCAT) to $1\,\mu atm$ (ASML - SOCAT). However, in the Newfoundland basin, the average difference is turned from $-17\,\mu atm$ (FREE - SOCAT) into $13\,\mu atm$ (ASML - SOCAT), which is associated with a larger absolute discrepancy of ASML and SOCAT.

DIC and alkalinity are two of the most important variables from which pCO_2 is derived (Section 4.2). Comparing them with observations provides more insights into the strengths and weaknesses of the modeled carbonate system than a comparison with pCO_2 observations alone. The FESOM-REcoM simulations represent higher surface DIC than GLODAP bottle observations (Lauvset et al., 2024a, gridded monthly-means) on average (Fig. 10a), with a global mean surface difference FREE-GLODAP of $6.46\,mmol\,C\,m^{-3}$ for DIC. Although fewer DIC observations are available than pCO_2 observations, similarities between the respective model-observations differences for DIC and pCO_2 can be recognized. For example, DIC in the model is lower in the tropical and subtropical Atlantic than GLODAP, and higher in the polar Atlantic. This is consistent with SOCAT pCO_2 observations in the same areas. The model-observation differences to GLODAP DIC and SOCAT pCO_2 are also consistent with each other in the north Pacific. The assimilation induces absolute changes in surface DIC of $6.33\,mmol\,C\,m^{-3}$ on global average, with regional differences in sign. These changes slightly reduce the mean absolute difference to the surface observations from $32.78\,mmol\,C\,m^{-3}$ to $32.15\,mmol\,C\,m^{-3}$, and yield a mixed picture of the improvement (Fig. 10b).

https://doi.org/10.5194/egusphere-2024-1750
Preprint. Discussion started: 20 June 2024

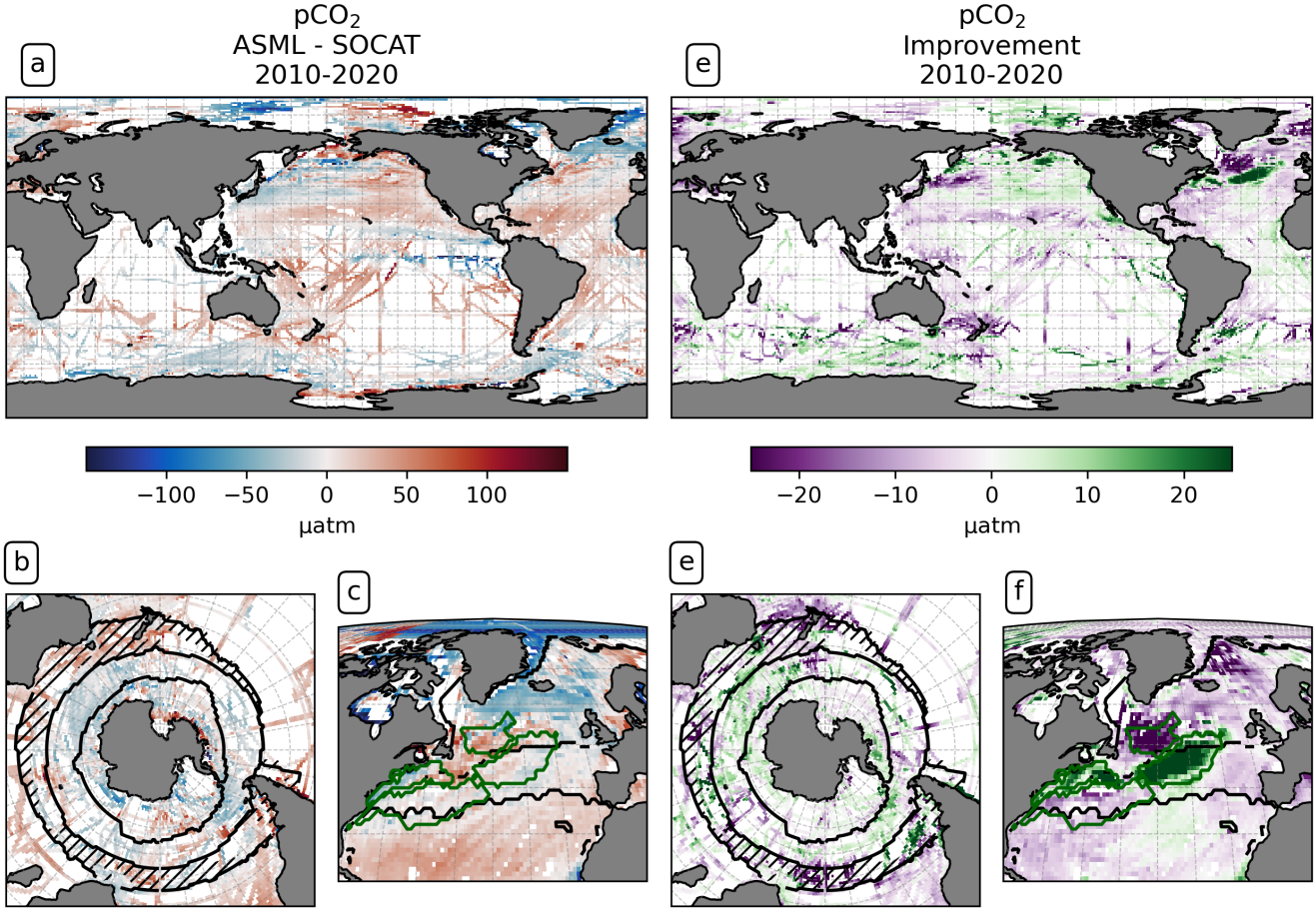

Figure 9. Partial pressure of CO_2 (pCO_2) at the surface averaged over the years 2010-2020. Panels (a-c) show the difference between FREE and SOCAT observations in (a) the global ocean, (b) Southern Ocean and (c) North Atlantic; panels (d-f) show the impact of the assimilation as 'improvement' relative to SOCAT observations computed from monthly mean pCO_2 in the same regions. Positive values (green color) denote a reduced difference to SOCAT.

https://doi.org/10.5194/egusphere-2024-1750
Preprint. Discussion started: 20 June 2024

While the trend in surface DIC due to anthropogenic input makes it necessary to compare the model with contemporaneous observations at the ocean surface, a comparison with climatological data is meaningful below a depth of approximately 200 m. In fact, the modeled global distribution of DIC at depth is overall similar to that in the GLODAP climatology (Fig. A9). For example, the model results and GLODAP data sets show that DIC is lowest in the isopycnals of the subtropical gyres ($2050-2150\,\mathrm{mmol\,C\,m^{-3}}$; Fig. A9a) and that DIC mostly increases with depth and is higher in the Pacific ($2420\,\mathrm{mmol\,C\,m^{-3}}$ at 1000 m in the North Pacific) than in the Atlantic ($2320\,\mathrm{mmol\,C\,m^{-3}}$ below 3000 m in the South Atlantic). Yet, depending on the ocean basin and depth, there can be both negative and positive differences between the simulations and the GLODAP climatology, which are in the order of $20\,\mathrm{mmol\,C\,m^{-3}}$ (Fig. A9c). On a global average, the assimilation leads to an increase in DIC between 200-600 m depth and a reduction of DIC between the surface and 200m, with the largest effect in the upper 400 m (Fig. A9b). This leads to an improved agreement with the GLODAP climatology, with the largest global mean improvement at a depth of 400 m ($2.5\,\mathrm{mmol\,C\,m^{-3}}$; (Fig. A9d). Below 1000 m depth, the global mean absolute difference FREE-ASML of DIC and alkalinity is only $1-2\,\mathrm{mmol\,m^{-3}}$ and is therefore substantially smaller than at the surface.

The comparison with GLODAP bottle alkalinity at the surface shows a similar spatial patterns as for DIC (see Fig. 10a and c). The magnitude of the bias is also comparable ($14\,\mathrm{mmol\,Alk\,m^{-3}}$). The global mean of the absolute difference ASML-FREE of surface alkalinity is $7.72\,\mathrm{mmol\,Alk\,m^{-3}}$. The assimilation leads to a reduction of the absolute difference of the model alkalinity to GLODAP from $34.34\,\mathrm{mmol\,Alk\,m^{-3}}$ to $32.60\,\mathrm{mmol\,Alk\,m^{-3}}$. Since the effects of physics assimilation on alkalinity and DIC are regionally consistent, regions of improved or deteriorated agreement with GLODAP often coincide for both variables (compare Fig. 10b and d). Since changes of DIC and alkalinity have an opposing effect on the CO_2 flux, it is likely that their correlation results in compensating effects. A linear estimate shows that the joint effect of DIC and alkalinity changes is responsible for a change in the CO_2 flux in the order of $1.22\,\mathrm{mmol\,C\,m^{-2}day^{-1}}$ on average, and, globally integrated, the assimilation-induced changes in DIC and alkalinity lead to an estimated net increase of the air-sea CO_2 flux by $0.50\,\mathrm{Pg\,C\,yr^{-1}}$. However, this linear offline estimate is subject to a large uncertainty.

The representation of chlorophyll by the model is of interest as a pCO_2-independent proxy for primary production. Surface chlorophyll reflects the phytoplankton state and biomass, and therefore, effects of the DA on the biological model state can be seen in the total surface chlorophyll concentration. A comparison of the modeled surface chlorophyll with remotely-sensed chlorophyll from OC-CCI reveals that the simulations capture the global distribution of chlorophyll well (Fig. 11). The simulations show the seasonal maxima in each hemisphere around one month earlier in the year (not shown). FREE features a higher surface chlorophyll concentration than OC-CCI by $0.02\,\mathrm{mg\,m^{-3}}$ on average, with low deviations in the tropics and an enhanced difference north of $30\,^{\circ}\mathrm{N}$ ($0.12\,\mathrm{mg\,m^{-3}}$) and south of $30\,^{\circ}\mathrm{S}$ ($0.24\,\mathrm{mg\,m^{-3}}$) (Fig. 11a). South of $30\,^{\circ}\mathrm{S}$, FREE is in better agreement with chlorophyll-a from Johnson et al.'s (2013) Southern Ocean specific chlorophyll product (Fig. 11a) than with OC-CCI data.

On global average, the assimilation slightly reduces the differences between model and OC-CCI data, from a global mean absolute difference of $0.31\,\mathrm{mg\,m^{-3}}$ to $0.29\,\mathrm{mg\,m^{-3}}$. The assimilation changes the chlorophyll concentration by an absolute value of $0.05\,\mathrm{mg\,m^{-3}}$ on average, which is 15% of the global mean absolute difference to OC-CCI. There are regions in which assimilation leads to a reduction in chlorophyll and thus to better agreement with the satellite products, for example in the

https://doi.org/10.5194/egusphere-2024-1750
Preprint. Discussion started: 20 June 2024

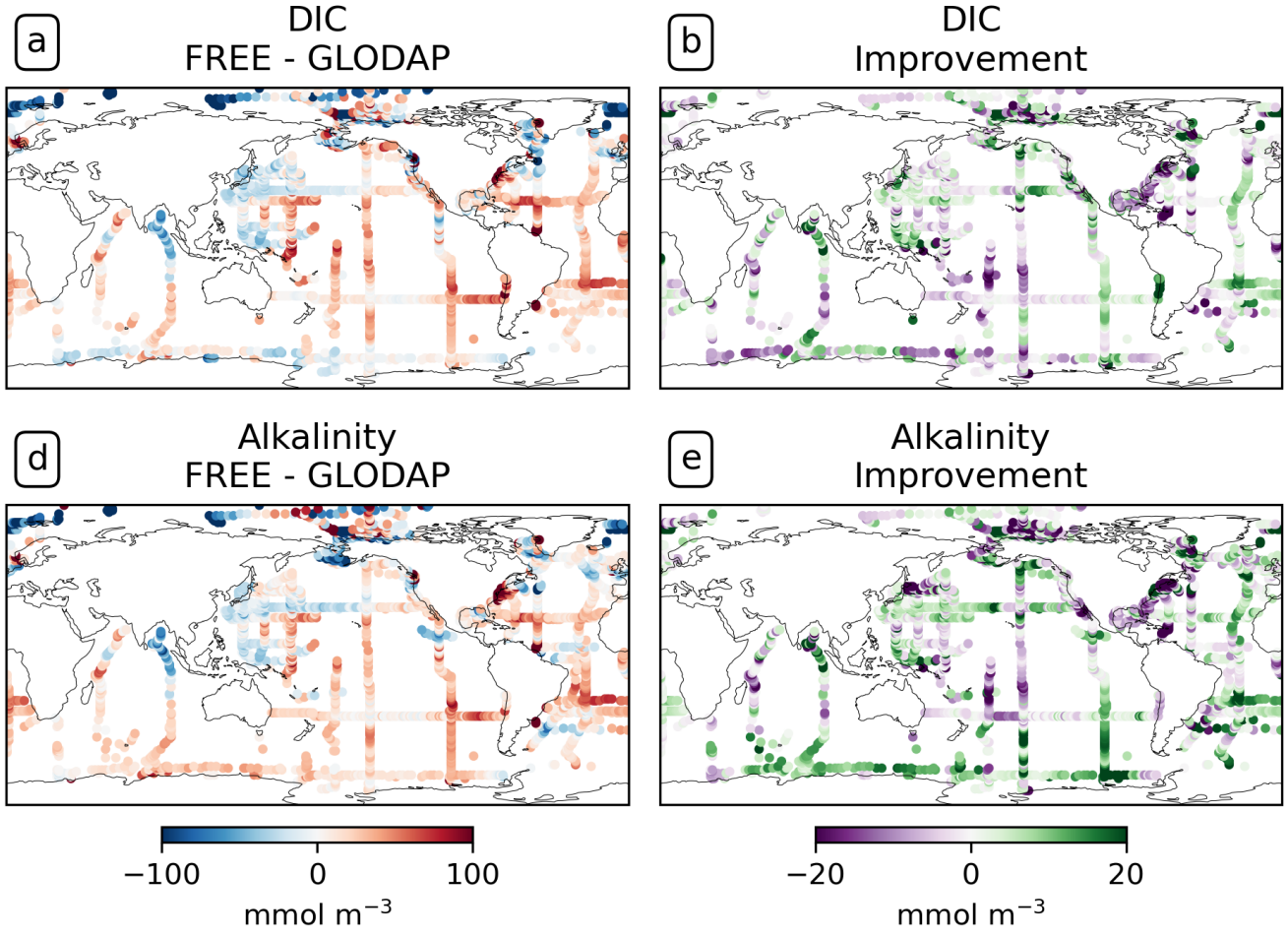

Figure 10. Comparison of the model result with surface DIC and alkalinity bottle observations from GLODAP over the years 2010 to 2020. (a) Difference of DIC between FREE and GLODAP. (b) Improvement of monthly surface DIC relative to GLODAP. (c and d) For alkalinity.

https://doi.org/10.5194/egusphere-2024-1750
Preprint. Discussion started: 20 June 2024

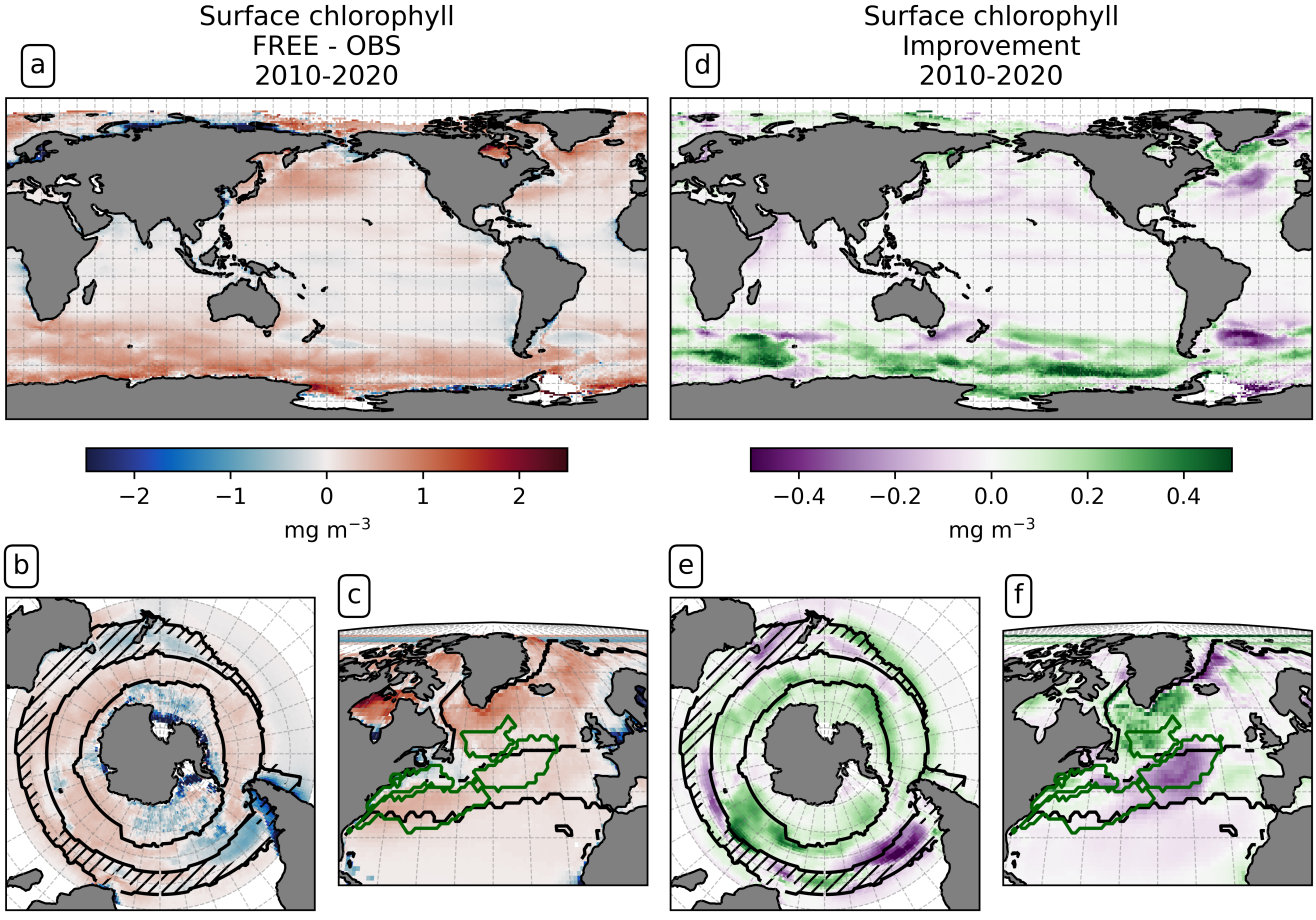

Figure 11. Surface chlorophyll averaged over the years 2010-2020: (a-c) difference between FREE and SOCAT observations in (a) the global ocean, (b) the Southern Ocean and (c) the North Atlantic; (d-f) impact of the assimilation as 'improvement' relative to the observations in the same regions. Panels (a, c, d) and (f) compare to monthly OC-CCI observations, panels (b) and (e) refer to the climatology for 1998-2019 by Johnson et al. (2013).

North Atlantic Subpolar Gyre and the Southern Ocean SPSS (Fig. 11b and e). In contrast, the model reacts to the DA with an increase in chlorophyll in the North Atlantic Central STSS and the Argentine Basin (Fig. 11b and f), which leads to poorer agreement.

5 Discussion

The assimilation of physics has different effects on BGC surface variables, though the major effects seem to be related to changes of SST (Section 4.3). Surface chlorophyll changes follow SST changes (Fig. 11 and Fig. 1), as the modeled phy-

https://doi.org/10.5194/egusphere-2024-1750
Preprint. Discussion started: 20 June 2024

toplankton growth is temperature-dependent (Gürses et al., 2023). The changes of surface DIC and alkalinity show similar spatial patterns with regional heterogeneity (Section 4.2), again with the major changes being coherent with the changes in SST (Fig. 1). Furthermore, the effects of the assimilation on DIC and on temperature in the upper 1000 m correlate regionally. Cooling at intermediate depth (Fig. 2b) is usually accompanied by higher DIC (Fig. A9), while warming near the surface co-occurs with reduced DIC. An overall more stable ocean stratification in the upper hundreds of meters explains why; on global average, the assimilation leads to lower DIC above 200 m and higher DIC between 200-600 m depth. In addition to changes in stability and mixing, the assimilation affects the distribution of DIC and alkalinity through changes in horizontal and vertical advection, with changes in the horizontal advection being about an order of magnitude larger than in the vertical. The horizontal distribution of surface DIC, alkalinity and SST is governed by latitudinal gradients and common pathways of advective transport, so that all of them undergo similar changes as the SST field is modified. The exception to this is the Southern Ocean STSS, where changes in the horizontal transport of DIC, alkalinity and temperature along contrasting surface gradients affect the respective variables differently (Section 4.2, Fig. A5, Fig. A6). The physics assimilation affects pCO_2 directly through the thermal effect, but also indirectly through changes of DIC and alkalinity, among other factors. Globally, changes in pCO_2 are dominated by changes in DIC and alkalinity, but regionally, also the thermal effect can be the largest, for example in the North Atlantic Newfoundland Basin (Fig. A10). While the DA dynamically induces changes in surface pCO_2 globally, the strongest effects on the air-sea CO_2 flux are at high latitudes, where the pCO_2 changes are amplified by high wind velocities.

The improvement in ocean physics overall leads to a more heterogeneous picture in biogeochemistry. While near-surface temperature and salinity fields are improved through DA almost everywhere, the global mean absolute difference of modeled surface pCO_2 to SOCAT remains similar in ASML compared to FREE, and this also applies to the model-observation differences for surface chlorophyll, DIC and alkalinity (Section 4.3). Where improvements in one BGC variable occur, these do not necessarily lead to consistent improvement in all BGC variables. For example, the representation of pCO_2 improves while that of chlorophyll deteriorates in the North Atlantic Central STSS (Fig. 11f and Fig. 9f). In the Southern SPSS, the reduction of modeled surface chlorophyll and the summer increase of pCO_2 in the Southern Ocean SPSS lead to a better agreement with observations, yet the available observations of DIC and alkalinity do not resolve the regional scales to evaluate the corresponding changes in these variables (Fig. 9, Fig. 10 and Fig. 11). One possible reason for improvement of model-data mismatch in one variable with worsening in another may lie in inconsistencies between the observational datasets. Another reason may be missing processes in the model or the use of constant BGC model parameters. Those parameters are responsible for linking changes between ecosystem variables and in reality, they vary across space and time depending on species composition in the ecosystem (Mamnun et al., 2023, Chapter 3).

The global air-sea CO_2 flux estimates of FREE and ASML fall in the range of previous model estimates and in the range of previous pCO_2 products (Fig. 4a and b) for the period 2010-2018, during which comparable estimates are available (DeVries et al., 2023). Thus, the overall impact of the DA on the air-sea CO_2 flux on a global scale is modest ($0.05\,\mathrm{Pg\,C\,dec^{-1}}$) compared to the differences between other estimates (e.g., a standard deviation of $0.20\,\mathrm{Pg\,C\,dec^{-1}}$ in DeVries et al., 2023). However, regionally, the effects of DA are more pronounced.

https://doi.org/10.5194/egusphere-2024-1750
Preprint. Discussion started: 20 June 2024

There are two other data assimilating BGC model approaches, namely ECCO-Darwin (global; Carroll et al., 2020)) and B-SOSE, which is restricted to the Southern Ocean (Verdy and Mazloff, 2017). Both approaches use Linearized Least Squares Optimization data assimilation methods (4D-var/adjoint and Green's function, Wunsch, 1996; Menemenlis et al., 2005). However, the largest difference to our study is probably that they assimilate BGC observations in addition to physical data. Thus, as expected, the effect on pCO_2 in our study is smaller (3%) than in ECCO-Darwin and B-SOSE where a reduction in pCO_2 model data misfit of 6% and 64% was reported, respectively (here given as quadratic misfit).

The global CO_2 flux is smaller in FESOM2.1-REcoM3-PDAF ($-2.73\,\mathrm{Pg\,C\,dec^{-1}}$) than in ECCO-Darwin ($-3.13\,\mathrm{Pg\,C\,dec^{-1}}$) (2010-2018). The global CO_2 flux in ASML is similar to FREE and does not drive the estimate closer towards the higher estimates of the ECCO-Darwin or the observation-based pCO_2-products ($-2.87\,\mathrm{Pg\,C\,dec^{-1}}$). Similarly, the trend and interannual variability of the CO_2 flux is hardly changed by the assimilation, suggesting that a flawed representation of ocean physics as an argument for the models underestimating the CO_2 flux trend is unlikely.

The discrepancy between the CO_2 flux estimates based on models and pCO_2-products is an area of active research and is not fully resolved (Friedlingstein et al., 2023; DeVries et al., 2023). On the one hand, model biases in the AMOC, in Southern Ocean ventilation and possibly biases in the surface ocean carbonate chemistry were suggested as reasons why models might underestimate the global mean CO_2 uptake in recent decades (Friedlingstein et al., 2023; Terhaar et al., 2024, 2022). On the other hand, the sparsity of observations is a concern for the pCO_2 products. According to one testbed simulation, the pCO_2 products reflect the global mean and the seasonal cycle relatively well, while the decadal variability may be overestimated (Gloege et al., 2021). An overestimation of the decadal trend, as suggested by Hauck et al. (2023b), could explain the high estimates of the pCO_2 products for the present-day global mean CO_2 flux. In contrast, for the North Atlantic, it was argued that pCO_2 is comparatively well constrained by observations in the last decade but not in the 1980s, which has an erroneous influence on the long-term trend (Pérez et al., 2024).

The effects of data assimilation on the CO_2 flux are most pronounced in the Southern Ocean STSS and SPSS in winter. Verdy and Mazloff (2017) also found the largest effects of assimilation on the CO_2 flux in this region. Although the region is of crucial importance for the global ocean carbon sink, it also has the greatest uncertainty due to the lack of ship-based winter observations (Friedlingstein et al., 2023; Hauck et al., 2020). In the last decade, the number of winter observations has increased due to the introduction of biogeochemical Argo floats (Johnson et al., 2017; Williams et al., 2017), although the float-based pCO_2 derived from pH measurements and estimated alkalinity is subject to higher uncertainty compared to direct pCO_2 measurements (Williams et al., 2017; Bakker et al., 2016). Machine learning approaches incorporating BGC Argo float observations suggest a stronger winter outgassing around Antarctica, particularly south of $50\,^{\circ}\mathrm{S}$ in the SPSS and ICE biomes, for 2015-2017 (Bushinsky et al., 2019; Gray et al., 2018). This results in a lower estimate of annual Southern Ocean CO_2 uptake in the float products. One suggestion in the literature was that model inadequacies in the representation of mixing and upwelling in the Southern Ocean could cause the discrepancy between float products and models (Gray et al., 2018). However, improvements in the modeled ocean physics and changes in mixing through data assimilation do not lead to not lead to closer agreement between the FESOM-REcoM estimate and the float products. In contrast, ASML shows even weaker winter outgassing and stronger summer uptake south of $50\,^{\circ}\mathrm{S}$ than FREE, which brings the FESOM-REcoM estimate further

https://doi.org/10.5194/egusphere-2024-1750
Preprint. Discussion started: 20 June 2024

away from the float products. However, ASML is brought close to B-SOSE in terms of winter outgassing in the Antarctic polar ocean (south of 60 °S) and winter uptake in the STSS (at 40 °S). Additionally, airborne CO_2 flux estimates and direct pCO_2 measurements stemming from a sail drone have questioned the estimates of winter outgassing based on the BGC floats, either attributing the high pCO_2 values to possible biases in the floats' measuring devices or to anomalously high pCO_2 in the years 2015-2016 (Long et al., 2021; Sutton et al., 2021). Based on the assumption of preindustrial steady state conditions, a larger natural CO_2 outgassing in the Southern Ocean needs to be compensated by other ocean regions (Gray et al., 2018). The regional differences caused by the data assimilation in the Southern Ocean and elsewhere largely balance out globally and appear to be shifts in the areas where outgassing occurs. These regional shifts follow shifts in sea surface temperature and the distribution of dissolved inorganic carbon (DIC) and alkalinity.

The comparably small effect of physics DA on the air-sea CO_2 flux suggests that the physical processes are already well-represented in FREE when compared to the uncertainties arising from the biogeochemistry model. The response of REcoM to changes in model physics might be small due to its variable stoichiometry, as the study by (Buchanan et al., 2018) indicated that dynamic biological functioning reduces the sensitivity of critical fields, like carbon, to physical changes. Furthermore, negative feedback effects between alkalinity, DIC, atmospheric pCO_2, and air-sea fluxes might reduce the overall response (Bunsen et al., 2024). While surface physics are well constrained in the ASML run, questions remain about the dynamics of the mixed layer and deep ocean. Experiments on decadal or longer time scales might be necessary to represent the adjustment of the ocean's carbon cycle to changes in the circulation (Cao et al., 2009). In ASML though, the effect on the CO_2 flux is already as strong in the first two years as at the end of the period, and it appears to be governed by interannual variability rather than showing a continuous adjustment. Despite the higher resolution in dynamic regions of the North Atlantic and the Arctic, strong currents and their exact locations, such as the North Atlantic Current and Antarctic Circumpolar Current, are challenging for the model to resolve. These are improved through the assimilation, which is the basis for realistically modeling biogeochemistry in these regions as well.

6 Conclusion

We apply data assimilation of temperature and salinity into a global ocean-biogeochemical model to improve the physical state for the years 2010-2020. The simulation is then assessed with regard to the effects on the biogeochemical variables. The experiments show that the effect of data assimilation (DA) on biogeochemical variables is mostly related to temperature changes. While the air-sea CO_2 flux and pCO_2 are directly affected by sea surface temperature, the DA also induced indirect changes to pCO_2 through dissolved inorganic carbon (DIC) and alkalinity. Globally integrated, these are more relevant for pCO_2 than the direct effect. Yet, which of these factors has a dominant effect on pCO_2 varies locally. The assimilation leads to changes in the horizontal advection of DIC and alkalinity, thereby regionally shifting areas of CO_2 outgassing and uptake. The largest effect on the air-sea CO_2 flux occurs in the Southern Ocean during winter. In the simulation with assimilation, the uptake south of 50 °S is increased, and the uptake northward of that (40-50 °S) is weakened. In this part of the ocean, the uncertainty in current estimates of CO_2 fluxes is particularly high. Furthermore, the assimilation has locally strong effects in the area of the

https://doi.org/10.5194/egusphere-2024-1750
Preprint. Discussion started: 20 June 2024

North Atlantic current. Overall, the uncertainty inherent to the biogeochemical model appears to be larger than the uncertainties induced through physical biases in the free running model. Locally, the changes in surface pCO_2, chlorophyll, alkalinity, and DIC caused by the assimilation are of the magnitude of 15-30% of the mean absolute model-observation difference. Yet, local improvements in one variable do not necessarily come along with improvements across other observed biogeochemical variables. Therefore, globally, physics DA does not generally improve the difference between the model and observations. In total, the effect of physics DA on the global ocean carbon uptake is small with $0.05\,\mathrm{Pg\,C\,yr^{-1}}$ compared to the spread between previous estimates of models, pCO_2 products and other DA estimates. While the assimilation of temperature and salinity improves the physical state, possible errors in the mixed layer depth and overturning circulation are not fully eliminated. Further biogeochemical variables are only indirectly affected. To this end, the additional assimilation of biogeochemical observations is an obvious next step to reduce the uncertainty stemming from the ecosystem model and to improve the model observation differences for biogeochemical variables.

Code and data availability. The code used to perform the free simulation and the data assimilation is available at 10.5281/zenodo.11495274. This code archive additionally contains a notebook to produce the manuscript figures from the model output. The processed model output data underlying the figures of this manuscript are available at 10.5281/zenodo.11495081.

Appendix A

Table A1. List of tracers in REcoM3

Tracers in REcoM3
Dissolved inorganic nitrogen and carbon (DIN, DIC)
Dissolved organic nitrogen and carbon (DON, DOC)
Alkalinity
Oxygen
Iron
Silicate
Intracellular concentrations of nitrogen, carbon, chlorophyll, and calcium in small phytoplankton (PhyN, PhyC, PhyChl, PhyCalc)
Intracellular concentrations of nitrogen, carbon, chlorophyll, and silicate in diatoms (DiaN, DiaC, DiaChl, DiaSi)
Intracellular concentrations of nitrogen and carbon in each of two zooplankton groups (HetN, HetC, Zoo2N, Zoo2C)
Two size classes of detritus for nitrogen, carbon, silicate, and calcium (DetN, DetC, DetSi, DetCalc; and DetZ2N, DetZ2C, DetZ2Si, DetZ2Calc)

https://doi.org/10.5194/egusphere-2024-1750
Preprint. Discussion started: 20 June 2024

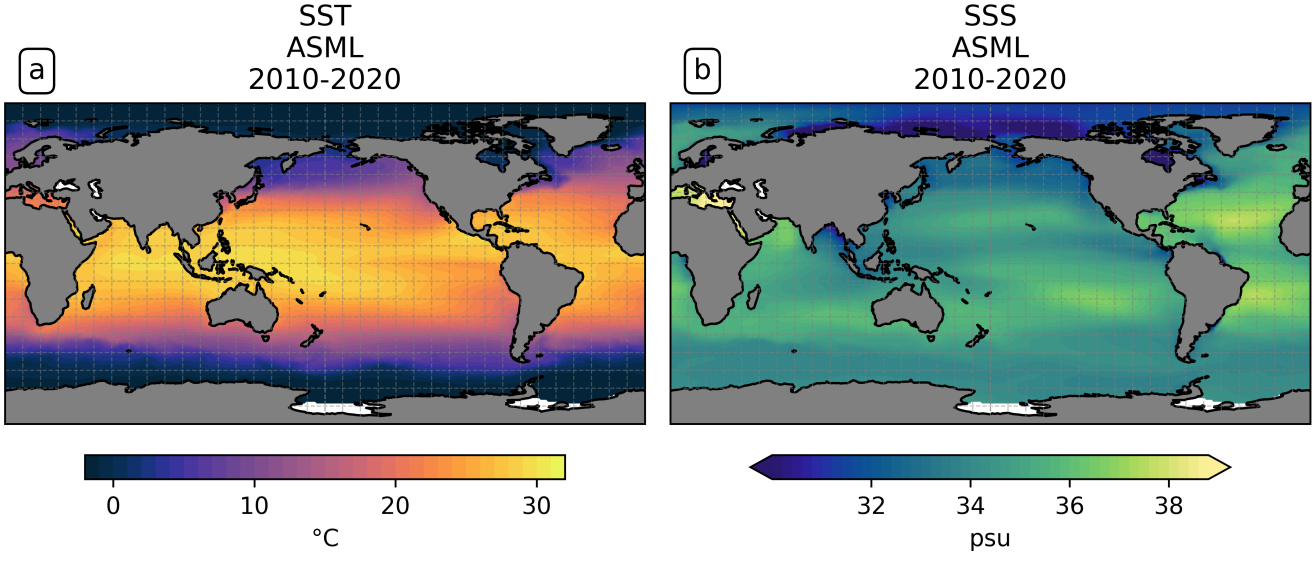

Figure A1. Time-mean sea surface (a) temperature and (b) salinity in ASML.

https://doi.org/10.5194/egusphere-2024-1750
Preprint. Discussion started: 20 June 2024

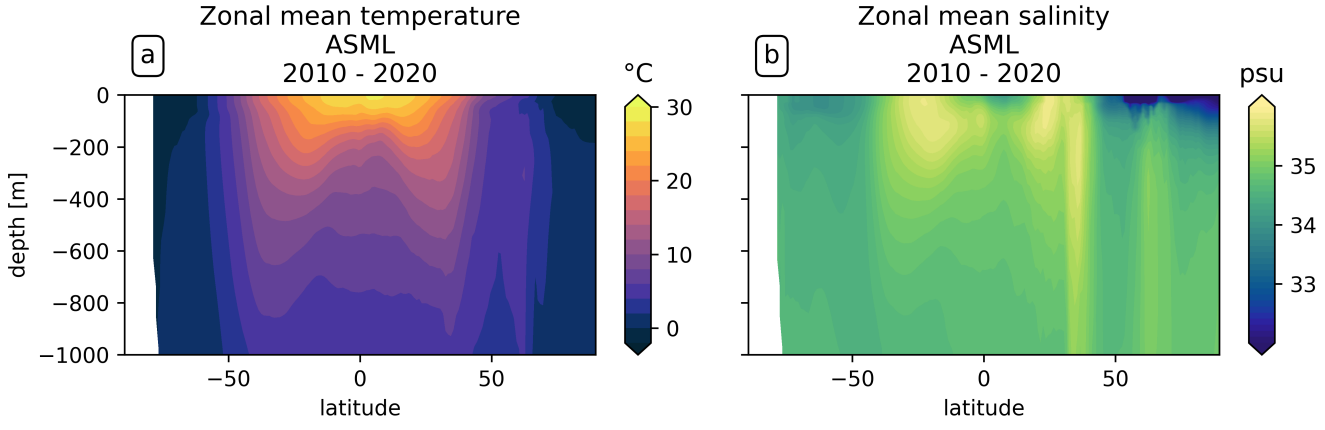

Figure A2. Zonally averaged time-mean (a) temperature and (b) salinity in ASML.

https://doi.org/10.5194/egusphere-2024-1750
Preprint. Discussion started: 20 June 2024

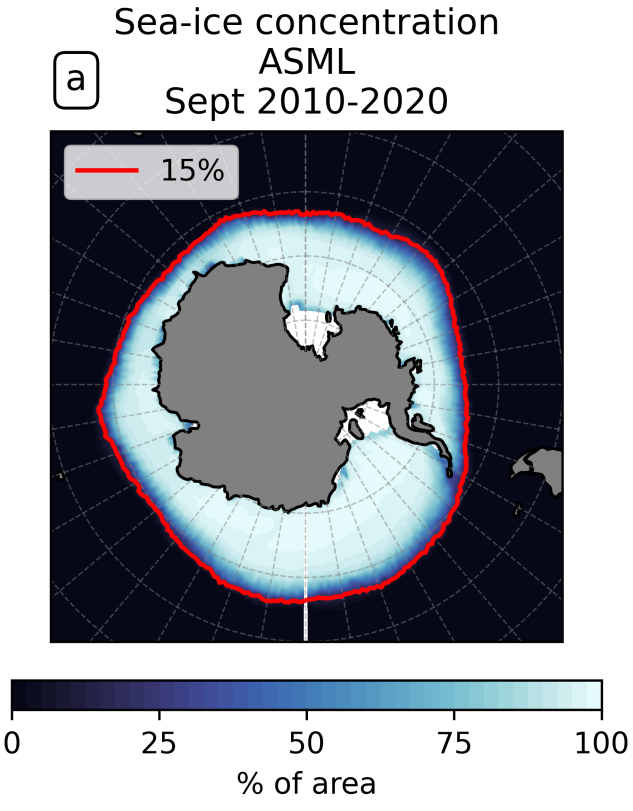

Figure A3. September mean antarctic sea-ice concentration in ASML.

https://doi.org/10.5194/egusphere-2024-1750
Preprint. Discussion started: 20 June 2024

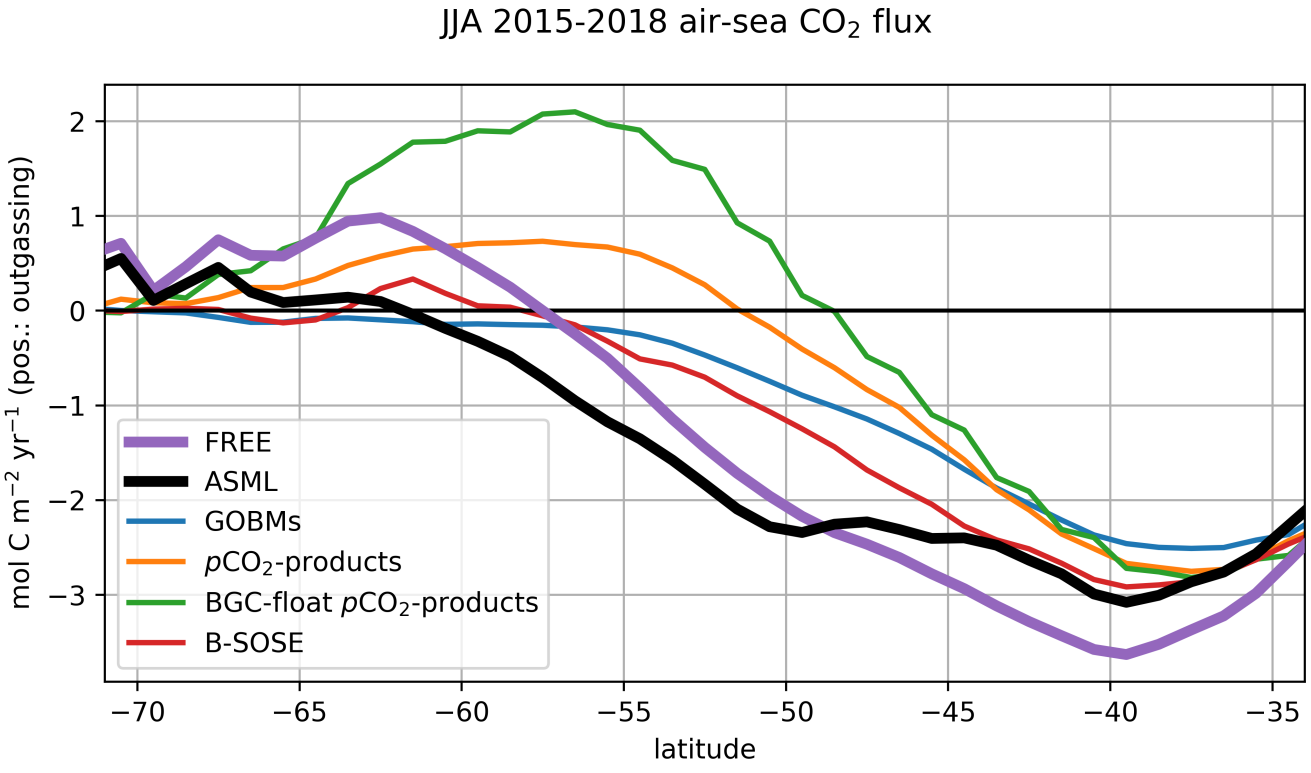

Figure A4. Zonally averaged winter (JJA) air-sea CO_2 flux in FREE, ASML and previous estimates (DeVries et al., 2023; Verdy and Mazloff, 2017).

https://doi.org/10.5194/egusphere-2024-1750
Preprint. Discussion started: 20 June 2024

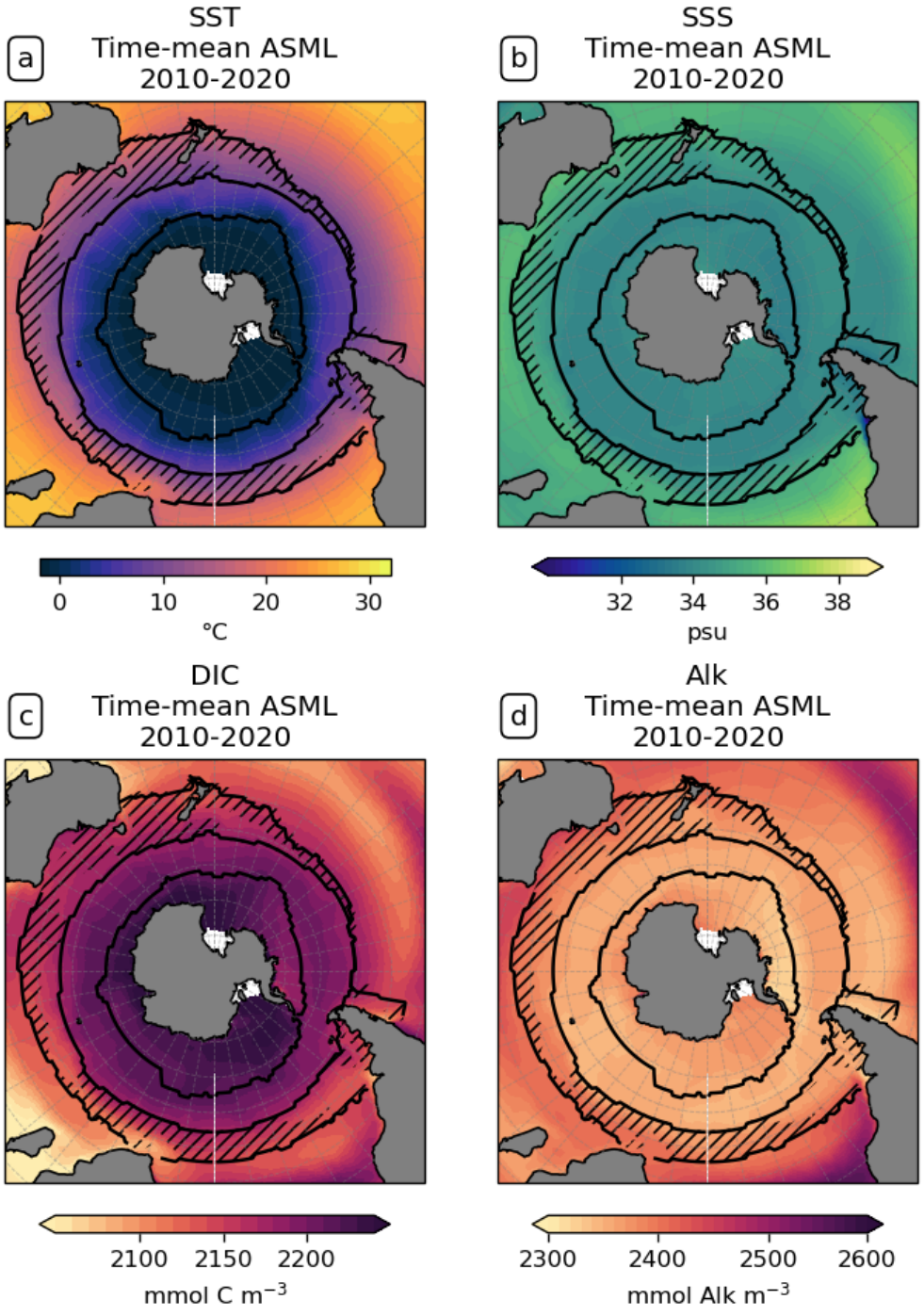

Figure A5. Southern Ocean time-mean sea surface in ASML, (a) temperature, (b) salinity, (c) dissolved inorganic carbon (DIC) and (d) alkalinity.

https://doi.org/10.5194/egusphere-2024-1750
Preprint. Discussion started: 20 June 2024

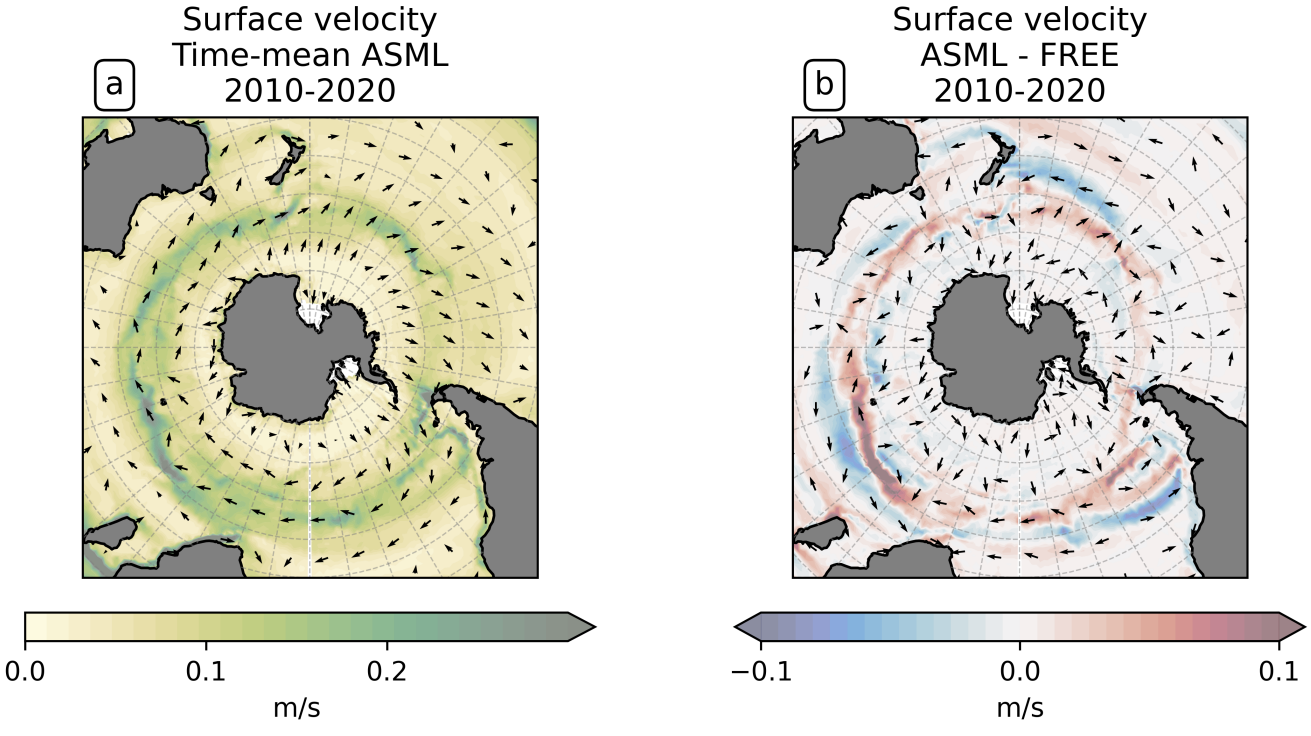

Figure A6. Surface velocities in the Southern Ocean, (a) time-mean in ASML and (b) difference ASML-FREE.

https://doi.org/10.5194/egusphere-2024-1750
Preprint. Discussion started: 20 June 2024

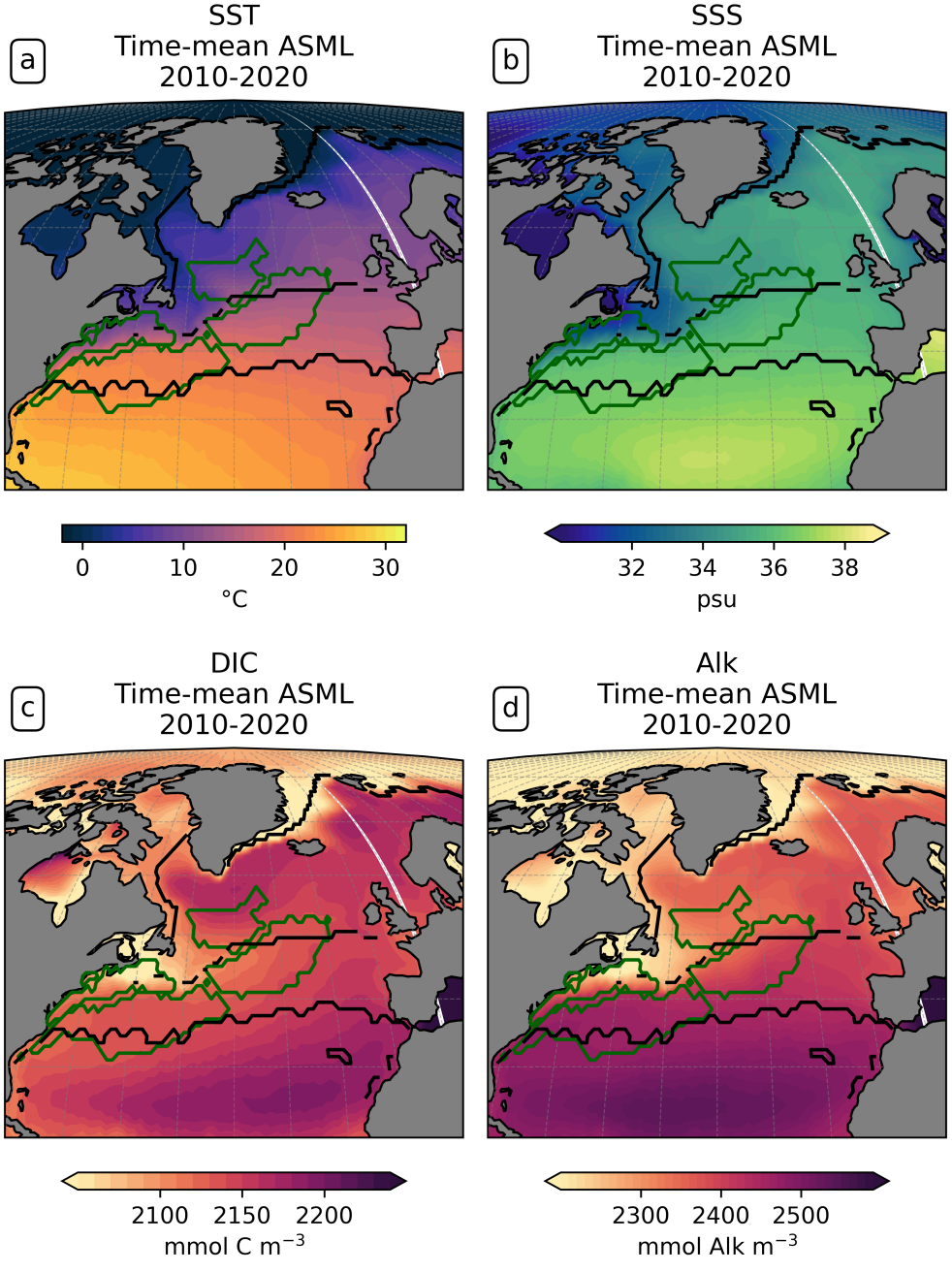

Figure A7. North Atlantic time-mean sea surface in ASML, (a) temperature, (b) salinity, (c) dissolved inorganic carbon (DIC) and (d) alkalinity.

https://doi.org/10.5194/egusphere-2024-1750
Preprint. Discussion started: 20 June 2024

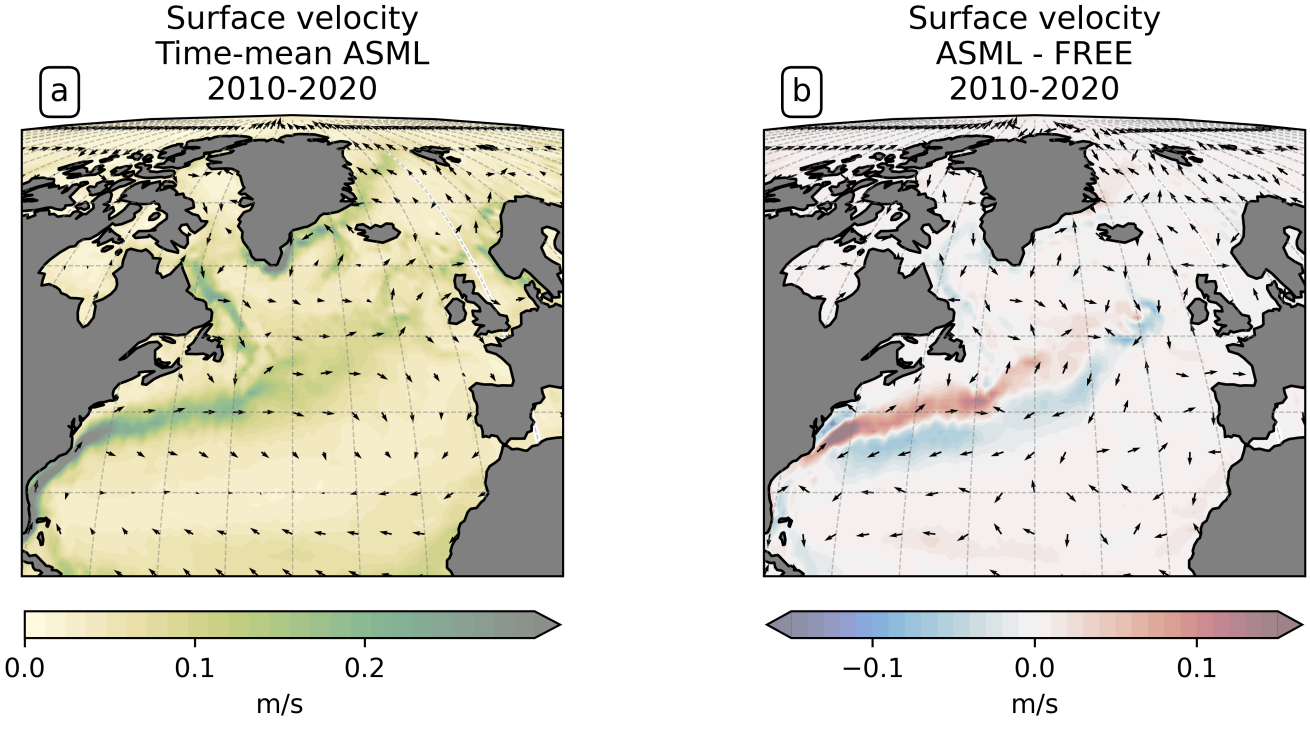

Figure A8. North Atlantic surface velocities, (a) time-mean in ASML and (b) difference ASML-FREE.

https://doi.org/10.5194/egusphere-2024-1750
Preprint. Discussion started: 20 June 2024

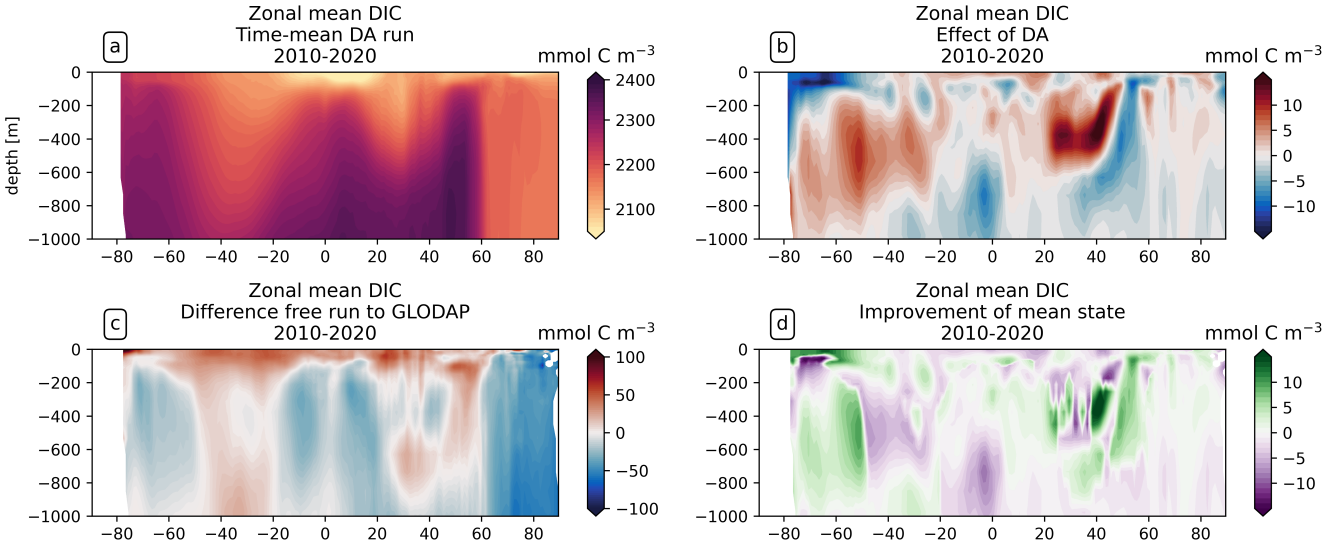

Figure A9. Zonally averaged dissolved inorganic carbon (DIC), (a) time-mean in ASML, (b) difference ASML-FREE, (c) difference FREE-OBS compared to the GLODAP climatology for DIC (Lauvset et al., 2016) and (d) improvement respective to the GLODAP climatology.

https://doi.org/10.5194/egusphere-2024-1750
Preprint. Discussion started: 20 June 2024

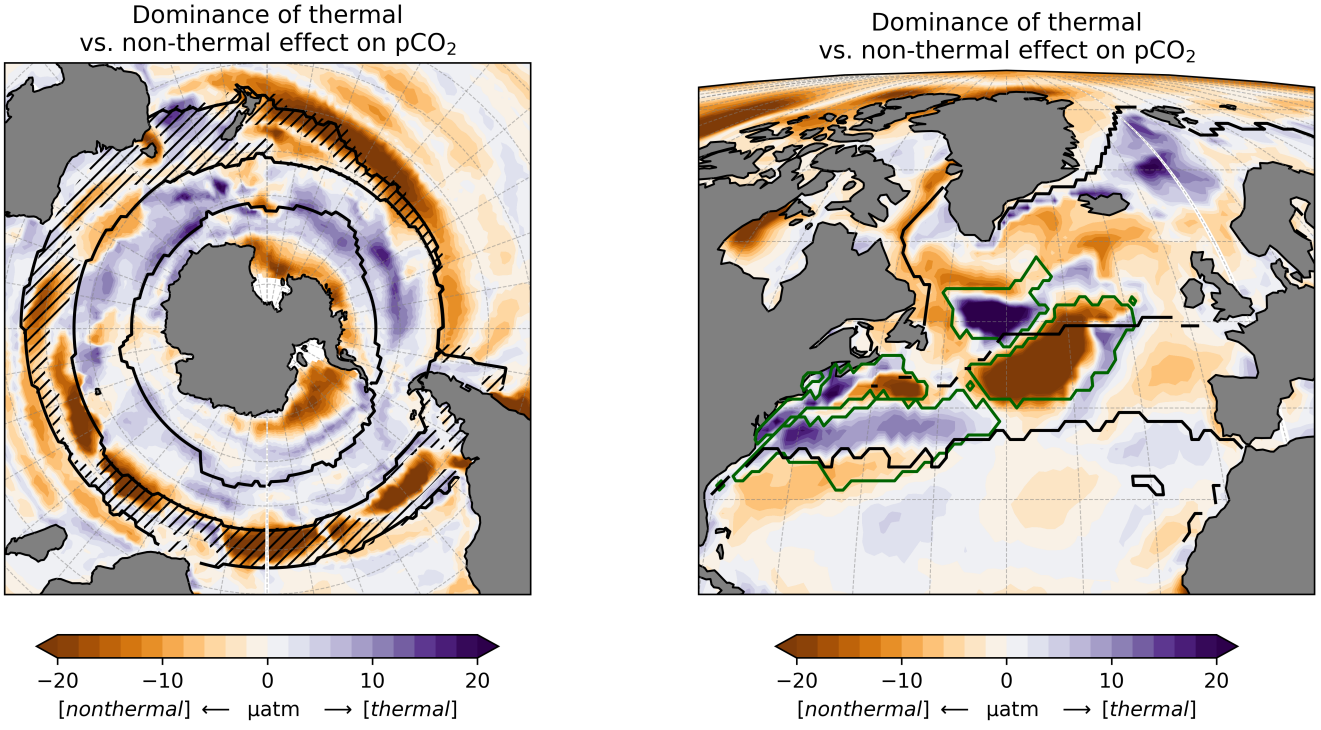

Figure A10. Linear offline estimate of the dominance of thermal versus the non-thermal effect through the assimilation on pCO_2.

https://doi.org/10.5194/egusphere-2024-1750
Preprint. Discussion started: 20 June 2024

Text A1: Velocity field A problem with deep equatorial vertical velocities is indicated by artifacts of the meridional overturning in ASML. Throughout the assimilation period, spurious, spatially limited and often deep overturning structures emerge, evolve through several months or years, and disappear in the tropical Indian, Pacific and Atlantic basin (not shown). Thereby, the surface overturning cell sometimes breaks apart where it should extend over the equator, exposing the bottom cell to the surface. One possible cause is the effect of data assimilation on the eddy parameterisation (Gent and Mcwilliams, 1990). The parameterised eddy activity is relevant for the dynamics in the deep ocean, and corrupting it can have a negative impact on the large-scale oceanic circulation, as described in Sidorenko (2004, Chapter 5.5 onwards) for a previous version of the ocean model FESOM.

https://doi.org/10.5194/egusphere-2024-1750
Preprint. Discussion started: 20 June 2024

Author contributions. JH and LN conceptualized the research idea and provided supervision of the work. FB worked on the code for the model binding, for which LN provided supervision, and performed formal analysis of the data and figure production. FB prepared the initial paper draft with conceptional inputs from all authors. All authors contributed to the review and editing of the final manuscript.

Competing interests. The authors declare that they have no conflict of interest.

Acknowledgements. We acknowledge the Global Carbon Project, which is responsible for the Global Carbon Budget and RECCAP and we thank the ocean modeling and fCO_2-mapping groups for producing and making available their model and fCO_2-product output; in particular Cara Nissen for providing the files. Further, we thank Longjiang Mu who provided code for a PDAF-model binding within the FESOM model family in order to modify it for our study. At last, we acknowledge the use of DeepL Free (DeepL SE, https://www.deepl.com/translator) for translations and of ChatGPT 3.5 (Open AI, https://chat.openai.com) to provide rewording suggestions for the text.

FB has received funding from the AWI INSPIRES programme, and JH from the Helmholtz Young Investigator Group Marine Carbon and Ecosystem Feedbacks in the Earth System (MarESys, Grant VHNG-1301), and from the European Research Council Starting Grant ERC2022-STG OceanPeak (Grant 101077209). The work reflects only the authors' view; the European Commission and their executive agency are not responsible for any use that may be made of the information the work contains.

https://doi.org/10.5194/egusphere-2024-1750
Preprint. Discussion started: 20 June 2024

References

Bakker, D. C. E., Pfeil, B., Landa, C. S., Metzl, N., O'Brien, K. M., Olsen, A., Smith, K., Cosca, C., Harasawa, S., Jones, S. D., Nakaoka, S., Nojiri, Y., Schuster, U., Steinhoff, T., Sweeney, C., Takahashi, T., Tilbrook, B., Wada, C., Wanninkhof, R., Alin, S. R., Balestrini, C. F., Barbero, L., Bates, N. R., Bianchi, A. A., Bonou, F., Boutin, J., Bozec, Y., Burger, E. F., Cai, W.-J., Castle, R. D., Chen, L., Chierici, M., Currie, K., Evans, W., Featherstone, C., Feely, R. A., Fransson, A., Goyet, C., Greenwood, N., Gregor, L., Hankin, S., Hardman-Mountford, N. J., Harlay, J., Hauck, J., Hoppema, M., Humphreys, M. P., Hunt, C. W., Huss, B., Ibánhez, J. S. P., Johannessen, T., Keeling, R., Kitidis, V., Körtzinger, A., Kozyr, A., Krasakopoulou, E., Kuwata, A., Landschützer, P., Lauvset, S. K., Lefèvre, N., Lo Monaco, C., Manke, A., Mathis, J. T., Merlivat, L., Millero, F. J., Monteiro, P. M. S., Munro, D. R., Murata, A., Newberger, T., Omar, A. M., Ono, T., Paterson, K., Pearce, D., Pierrot, D., Robbins, L. L., Saito, S., Salisbury, J., Schlitzer, R., Schneider, B., Schweitzer, R., Sieger, R., Skjelvan, I., Sullivan, K. F., Sutherland, S. C., Sutton, A. J., Tadokoro, K., Telszewski, M., Tuma, M., van Heuven, S. M. A. C., Vandemark, D., Ward, B., Watson, A. J., and Xu, S.: A multi-decade record of high-quality fCO_2 data in version 3 of the Surface Ocean CO_2 Atlas (SOCAT), Earth System Science Data, 8, 383–413, https://doi.org/10.5194/essd-8-383-2016, 2016.

Bakker, D. C. E., Alin, S. R., Bates, N., Becker, M., Feely, R. A., Gkritzalis, T., Jones, S. D., Kozyr, A., Lauvset, S. K., Metzl, N., Munro, D. R., Nakaoka, S.-i., Nojiri, Y., O'Brien, K. M., Olsen, A., Pierrot, D., Rehder, G., Steinhoff, T., Sutton, A. J., Sweeney, C., Tilbrook, B., Wada, C., Wanninkhof, R., Akl, J., Barbero, L., Beatty, C. M., Berghoff, C. F., Bittig, H. C., Bott, R., Burger, E. F., Cai, W.-J., Castaño Primo, R., Corredor, J. E., Cronin, M., De Carlo, E. H., DeGrandpre, M. D., Dietrich, C., Drennan, W. M., Emerson, S. R., Enochs, I. C., Enyo, K., Epherra, L., Evans, W., Fiedler, B., Fontela, M., Frangoulis, C., Gehrung, M., Giannoudi, L., Glockzin, M., Hales, B., Howden, S. D., Ibánhez, J. S. P., Kamb, L., Körtzinger, A., Lefèvre, N., Lo Monaco, C., Lutz, V. A., Macovei, V. A., Maenner Jones, S., Manalang, D., Manzello, D. P., Metzl, N., Mickett, J., Millero, F. J., Monacci, N. M., Morell, J. M., Musielewicz, S., Neill, C., Newberger, T., Newton, J., Noakes, S., Ólafsdóttir, S. R., Ono, T., Osborne, J., Padín, X. A., Paulsen, M., Perivoliotis, L., Petersen, W., Petihakis, G., Plueddemann, A. J., Rodriguez, C., Rutgersson, A., Sabine, C. L., Salisbury, J. E., Schlitzer, R., Skjelvan, I., Stamataki, N., Sullivan, K. F., Sutherland, S. C., T'Jampens, M., Tadokoro, K., Tanhua, T., Telszewski, M., Theetaert, H., Tomlinson, M., Vandemark, D., Velo, A., Voynova, Y. G., Weller, R. A., Whitehead, C., and Wimart-Rousseau, C.: Surface Ocean CO_2 Atlas Database Version 2023 (SOCATv2023) (NCEI Accession 0278913), https://doi.org/10.25921/r7xa-bt92, 2023.

Ballantyne, A. P., Alden, C. B., Miller, J. B., Tans, P. P., and White, J. W. C.: Increase in observed net carbon dioxide uptake by land and oceans during the past 50 years, Nature, 488, 70–72, https://doi.org/10.1038/nature11299, 2012.

Boutin, J., Vergely, J.-L., Reul, N., Catany, R., Koehler, J., Martin, A., Rouffi, F., Arias, M., Chakroun, M., Corato, G., et al.: ESA Sea Surface Salinity Climate Change Initiative (Sea_Surface_Salinity_cci): Weekly and Monthly Sea Surface Salinity Product, v03.21, from 2010 to 2020, NERC EDS Centre for Environmental Data Analysis, http://dx.doi.org/10.5285/5920a2c77e3c45339477acd31ce62c3c, 2021.

Brix, H., Menemenlis, D., Hill, C., Dutkiewicz, S., Jahn, O., Wang, D., Bowman, K., and Zhang, H.: Using Green's Functions to initialize and adjust a global, eddying ocean biogeochemistry general circulation model, Ocean Modelling, 95, 1–14, https://doi.org/10.1016/j.ocemod.2015.07.008, 2015.

Buchanan, P. J., Matear, R. J., Chase, Z., Phipps, S. J., and Bindoff, N. L.: Dynamic Biological Functioning Important for Simulating and Stabilizing Ocean Biogeochemistry, Global Biogeochemical Cycles, 32, 565–593, https://doi.org/10.1002/2017GB005753, 2018.

Bunsen, F., Nissen, C., and Hauck, J.: The Impact of Recent Climate Change on the Global Ocean Carbon Sink, Geophysical Research Letters, 51, e2023GL107 030, https://doi.org/10.1029/2023GL107030, 2024.

https://doi.org/10.5194/egusphere-2024-1750
Preprint. Discussion started: 20 June 2024

Bushinsky, S. M., Landschützer, P., Rödenbeck, C., Gray, A. R., Baker, D., Mazloff, M. R., Resplandy, L., Johnson, K. S., and Sarmiento, J. L.: Reassessing Southern Ocean Air-Sea CO2 Flux Estimates With the Addition of Biogeochemical Float Observations, Global Biogeochemical Cycles, 33, 1370–1388, https://doi.org/10.1029/2019GB006176, 2019.

Cao, L., Eby, M., Ridgwell, A., Caldeira, K., Archer, D., Ishida, A., Joos, F., Matsumoto, K., Mikolajewicz, U., Mouchet, A., Orr, J. C., Plattner, G.-K., Schlitzer, R., Tokos, K., Totterdell, I., Tschumi, T., Yamanaka, Y., and Yool, A.: The role of ocean transport in the uptake of anthropogenic CO2, Biogeosciences, 6, 375–390, https://doi.org/10.5194/bg-6-375-2009, 2009.

Carroll, D., Menemenlis, D., Adkins, J. F., Bowman, K. W., Brix, H., Dutkiewicz, S., Fenty, I., Gierach, M. M., Hill, C., Jahn, O., Landschützer, P., Lauderdale, J. M., Liu, J., Manizza, M., Naviaux, J. D., Rödenbeck, C., Schimel, D. S., Van der Stocken, T., and Zhang, H.: The ECCO-Darwin Data-Assimilative Global Ocean Biogeochemistry Model: Estimates of Seasonal to Multidecadal Surface Ocean pCO2 and Air-Sea CO2 Flux, Journal of Advances in Modeling Earth Systems, 12, e2019MS001 888, https://doi.org/10.1029/2019MS001888, 2020.

Chapman, C. C., Lea, M.-A., Meyer, A., Sallée, J.-B., and Hindell, M.: Defining Southern Ocean fronts and their influence on biological and physical processes in a changing climate, Nature Climate Change, 10, 209–219, https://doi.org/10.1038/s41558-020-0705-4, 2020.

CMEMS Marine Data Store: Operational Sea Surface Temperature and Ice Analysis (OSTIA), https://doi.org/10.48670/moi-00165.

Crisp, D., Dolman, H., Tanhua, T., McKinley, G. A., Hauck, J., Bastos, A., Sitch, S., Eggleston, S., and Aich, V.: How Well Do We Understand the Land-Ocean-Atmosphere Carbon Cycle?, Reviews of Geophysics, 60, e2021RG000 736, https://doi.org/10.1029/2021RG000736, 2022.

Danilov, S., Sidorenko, D., Wang, Q., and Jung, T.: The Finite-volumE Sea ice–Ocean Model (FESOM2), Geoscientific Model Development, 10, 765–789, https://doi.org/10.5194/gmd-10-765-2017, 2017.

Davila, X., Gebbie, G., Brakstad, A., Lauvset, S. K., McDonagh, E. L., Schwinger, J., and Olsen, A.: How Is the Ocean Anthropogenic Carbon Reservoir Filled?, Global Biogeochemical Cycles, 36, e2021GB007 055, https://doi.org/10.1029/2021GB007055, 2022.

Denvil-Sommer, A., Gehlen, M., and Vrac, M.: Observation system simulation experiments in the Atlantic Ocean for enhanced surface ocean pCO2 reconstructions, Ocean Science, 17, 1011–1030, https://doi.org/10.5194/os-17-1011-2021, 2021.

DeVries, T., Yamamoto, K., Wanninkhof, R., Gruber, N., Hauck, J., Müller, J. D., Bopp, L., Carroll, D., Carter, B., Chau, T.-T.-T., Doney, S. C., Gehlen, M., Gloege, L., Gregor, L., Henson, S., Kim, J. H., Iida, Y., Ilyina, T., Landschützer, P., Le Quéré, C., Munro, D., Nissen, C., Patara, L., Pérez, F. F., Resplandy, L., Rodgers, K. B., Schwinger, J., Séférian, R., Sicardi, V., Terhaar, J., Triñanes, J., Tsujino, H., Watson, A., Yasunaka, S., and Zeng, J.: Magnitude, Trends, and Variability of the Global Ocean Carbon Sink From 1985 to 2018, Global Biogeochemical Cycles, 37, e2023GB007 780, https://doi.org/10.1029/2023GB007780, 2023.

Doney, S. C., Lindsay, K., Caldeira, K., Campin, J.-M., Drange, H., Dutay, J.-C., Follows, M., Gao, Y., Gnanadesikan, A., Gruber, N., Ishida, A., Joos, F., Madec, G., Maier-Reimer, E., Marshall, J. C., Matear, R. J., Monfray, P., Mouchet, A., Najjar, R., Orr, J. C., Plattner, G.-K., Sarmiento, J., Schlitzer, R., Slater, R., Totterdell, I. J., Weirig, M.-F., Yamanaka, Y., and Yool, A.: Evaluating global ocean carbon models: The importance of realistic physics, Global Biogeochemical Cycles, 18, https://doi.org/10.1029/2003GB002150, 2004.

Doney, S. C., Lima, I., Feely, R. A., Glover, D. M., Lindsay, K., Mahowald, N., Moore, J. K., and Wanninkhof, R.: Mechanisms governing interannual variability in upper-ocean inorganic carbon system and air–sea CO2 fluxes: Physical climate and atmospheric dust, Deep Sea Research Part II: Topical Studies in Oceanography, 56, 640–655, https://doi.org/10.1016/j.dsr2.2008.12.006, 2009.

Donlon, C., Martin, M., Stark, J., Roberts-Jones, J., Fiedler, E., and Wimmer, W.: The Operational Sea Surface Temperature and Sea Ice Analysis (OSTIA) system, Remote Sensing of the Environment, https://doi.org/10.1016/j.rse.2010.10.017, 2012.

https://doi.org/10.5194/egusphere-2024-1750
Preprint. Discussion started: 20 June 2024

EUMETSAT: OSI SAF Global medium resolution sea ice concentration climate data record 2002-2020 (v3.0), Ocean and Sea Ice Satellite Application Facility, https://doi.org/10.15770/EUM_SAF_OSI_0015, 2022.

Fay, A. R. and McKinley, G. A.: Global open-ocean biomes: mean and temporal variability, Earth System Science Data, 6, 273–284, https://doi.org/10.5194/essd-6-273-2014, 2014.

Fennel, K., Mattern, J. P., Doney, S. C., Bopp, L., Moore, A. M., Wang, B., and Yu, L.: Ocean biogeochemical modelling, Nature Reviews Methods Primers, 2, 1–21, https://doi.org/10.1038/s43586-022-00154-2, 2022.

Fransner, F., Counillon, F., Bethke, I., Tjiputra, J., Samuelsen, A., Nummelin, A., and Olsen, A.: Ocean Biogeochemical Predictions—Initialization and Limits of Predictability, Frontiers in Marine Science, 7, 508 048, https://doi.org/10.3389/fmars.2020.00386, 2020.

Friedlingstein, P., O'Sullivan, M., Jones, M. W., Andrew, R. M., Bakker, D. C. E., Hauck, J., Landschützer, P., Le Quéré, C., Luijkx, I. T., Peters, G. P., Peters, W., Pongratz, J., Schwingshackl, C., Sitch, S., Canadell, J. G., Ciais, P., Jackson, R. B., Alin, S. R., Anthoni, P., Barbero, L., Bates, N. R., Becker, M., Bellouin, N., Decharme, B., Bopp, L., Brasika, I. B. M., Cadule, P., Chamberlain, M. A., Chandra, N., Chau, T.-T.-T., Chevallier, F., Chini, L. P., Cronin, M., Dou, X., Enyo, K., Evans, W., Falk, S., Feely, R. A., Feng, L., Ford, D. J., Gasser, T., Ghattas, J., Gkritzalis, T., Grassi, G., Gregor, L., Gruber, N., Gürses, Ö., Harris, I., Hefner, M., Heinke, J., Houghton, R. A., Hurtt, G. C., Iida, Y., Ilyina, T., Jacobson, A. R., Jain, A., Jarníková, T., Jersild, A., Jiang, F., Jin, Z., Joos, F., Kato, E., Keeling, R. F., Kennedy, D., Klein Goldewijk, K., Knauer, J., Korsbakken, J. I., Körtzinger, A., Lan, X., Lefèvre, N., Li, H., Liu, J., Liu, Z., Ma, L., Marland, G., Mayot, N., McGuire, P. C., McKinley, G. A., Meyer, G., Morgan, E. J., Munro, D. R., Nakaoka, S.-I., Niwa, Y., O'Brien, K. M., Olsen, A., Omar, A. M., Ono, T., Paulsen, M., Pierrot, D., Pocock, K., Poulter, B., Powis, C. M., Rehder, G., Resplandy, L., Robertson, E., Rödenbeck, C., Rosan, T. M., Schwinger, J., Séférian, R., Smallman, T. L., Smith, S. M., Sospedra-Alfonso, R., Sun, Q., Sutton, A. J., Sweeney, C., Takao, S., Tans, P. P., Tian, H., Tilbrook, B., Tsujino, H., Tubiello, F., van der Werf, G. R., van Ooijen, E., Wanninkhof, R., Watanabe, M., Wimart-Rousseau, C., Yang, D., Yang, X., Yuan, W., Yue, X., Zaehle, S., Zeng, J., and Zheng, B.: Global Carbon Budget 2023, Earth System Science Data, 15, 5301–5369, https://doi.org/10.5194/essd-15-5301-2023, 2023.

Gaspari, G. and Cohn, S. E.: Construction of correlation functions in two and three dimensions, Quarterly Journal of the Royal Meteorological Society, 125, 723–757, https://doi.org/10.1002/qj.49712555417, 1999.

Gent, P. R. and Mcwilliams, J. C.: Isopycnal Mixing in Ocean Circulation Models, Journal of Physical Oceanography, 20, 150–155, https://doi.org/10.1175/1520-0485(1990)020<0150:IMIOCM>2.0.CO;2, 1990.

Gerber, M., Joos, F., Vázquez-Rodríguez, M., Touratier, F., and Goyet, C.: Regional air-sea fluxes of anthropogenic carbon inferred with an Ensemble Kalman Filter, Global Biogeochemical Cycles, 23, https://doi.org/10.1029/2008GB003247, 2009.

Gloege, L., McKinley, G. A., Landschützer, P., Fay, A. R., Frölicher, T. L., Fyfe, J. C., Ilyina, T., Jones, S., Lovenduski, N. S., Rodgers, K. B., Schlunegger, S., and Takano, Y.: Quantifying Errors in Observationally Based Estimates of Ocean Carbon Sink Variability, Global Biogeochemical Cycles, 35, e2020GB006 788, https://doi.org/10.1029/2020GB006788, 2021.

Good, S., Fiedler, E., Mao, C., Martin, M., Maycock, A., Reid, R., Roberts-Jones, J., Searle, T., Waters, J., While, J., and Worsfold, M.: The Current Configuration of the OSTIA System for Operational Production of Foundation Sea Surface Temperature and Ice Concentration Analyses, Remote Sens., 12, 720, https://doi.org/10.3390/rs12040720, 2020.

Good, S. A., Martin, M. J., and Rayner, N. A.: EN4: Quality Controlled Ocean Temperature and Salinity Profiles and Monthly Objective Analyses with Uncertainty Estimates, Journal of Geophysical Research: Oceans, https://doi.org/10.1002/2013JC009067, 2013.

Gray, A. R., Johnson, K. S., Bushinsky, S. M., Riser, S. C., Russell, J. L., Talley, L. D., Wanninkhof, R., Williams, N. L., and Sarmiento, J. L.: Autonomous Biogeochemical Floats Detect Significant Carbon Dioxide Outgassing in the High-Latitude Southern Ocean, Geophysical Research Letters, 45, 9049–9057, https://doi.org/10.1029/2018GL078013, 2018.

https://doi.org/10.5194/egusphere-2024-1750
Preprint. Discussion started: 20 June 2024

Gruber, N., Gloor, M., Fletcher, S. E. M., Doney, S. C., Dutkiewicz, S., Follows, M. J., Gerber, M., Jacobson, A. R., Joos, F., Lindsay, K., Menemenlis, D., Mouchet, A., Müller, S. A., Sarmiento, J. L., and Takahashi, T.: Oceanic sources, sinks, and transport of atmospheric CO2, Global Biogeochemical Cycles, 23, https://doi.org/10.1029/2008GB003349, 2009.

Gürses, O., Oziel, L., Karakuş, O., Sidorenko, D., Völker, C., Ye, Y., Zeising, M., Butzin, M., and Hauck, J.: Ocean biogeochemistry in the coupled ocean–sea ice–biogeochemistry model FESOM2.1–REcoM3, Geoscientific Model Development, 16, 4883–4936, https://doi.org/10.5194/gmd-16-4883-2023, 2023.

Hauck, J., Völker, C., Wang, T., Hoppema, M., Losch, M., and Wolf-Gladrow, D. A.: Seasonally Different Carbon Flux Changes in the Southern Ocean in Response to the Southern Annular Mode, Global Biogeochemical Cycles, 27, 1236–1245, https://doi.org/10.1002/2013GB004600, 2013.

Hauck, J., Zeising, M., Le Quéré, C., Gruber, N., Bakker, D. C. E., Bopp, L., Chau, T. T. T., Gürses, Ö., Ilyina, T., Landschützer, P., Lenton, A., Resplandy, L., Rödenbeck, C., Schwinger, J., and Séférian, R.: Consistency and Challenges in the Ocean Carbon Sink Estimate for the Global Carbon Budget, Frontiers in Marine Science, 7, 571 720, https://doi.org/10.3389/fmars.2020.571720, 2020.

Hauck, J., Gregor, L., Nissen, C., Patara, L., Hague, M., Mongwe, P., Bushinsky, S., Doney, S. C., Gruber, N., Le Quéré, C., Manizza, M., Mazloff, M., Monteiro, P. M. S., and Terhaar, J.: The Southern Ocean Carbon Cycle 1985–2018: Mean, Seasonal Cycle, Trends, and Storage, Global Biogeochemical Cycles, 37, e2023GB007 848, https://doi.org/10.1029/2023GB007848, 2023a.

Hauck, J., Nissen, C., Landschützer, P., Rödenbeck, C., Bushinsky, S., and Olsen, A.: Sparse observations induce large biases in estimates of the global ocean CO2 sink: an ocean model subsampling experiment, Philosophical Transactions of the Royal Society A, 381, 20220 063, https://doi.org/10.1098/rsta.2022.0063, 2023b.

Hohn, S.: Coupling and decoupling of biogeochemical cycles in marine ecosystems, Ph.D. thesis, University of Bremen, 2008.

Johnson, K. S., Plant, J. N., Coletti, L. J., Jannasch, H. W., Sakamoto, C. M., Riser, S. C., Swift, D. D., Williams, N. L., Boss, E., Haëntjens, N., Talley, L. D., and Sarmiento, J. L.: Biogeochemical sensor performance in the SOCCOM profiling float array, Journal of Geophysical Research: Oceans, 122, 6416–6436, https://doi.org/10.1002/2017JC012838, 2017.

Johnson, R., Strutton, P. G., Wright, S. W., McMinn, A., and Meiners, K. M.: Three Improved Satellite Chlorophyll Algorithms for the Southern Ocean, Journal of Geophysical Research: Oceans, 118, 3694–3703, https://doi.org/10.1002/jgrc.20270, 2013.

Jones, S. D., Le Quéré, C., and Rödenbeck, C.: Autocorrelation characteristics of surface ocean pCO2and air-sea CO2 fluxes, Global Biogeochemical Cycles, 26, https://doi.org/10.1029/2010GB004017, 2012.

Joos, F. and Spahni, R.: Rates of change in natural and anthropogenic radiative forcing over the past 20,000 years, Proceedings of the National Academy of Sciences, 105, 1425–1430, https://doi.org/10.1073/pnas.0707386105, 2008.

Karakuş, O., Völker, C., Iversen, M., Hagen, W., Wolf-Gladrow, D., Fach, B., and Hauck, J.: Modeling the Impact of Macrozooplankton on Carbon Export Production in the Southern Ocean, Journal of Geophysical Research: Oceans, 126, e2021JC017 315, https://doi.org/10.1029/2021JC017315, 2021.

Keppler, L. and Landschützer, P.: Regional wind variability modulates the Southern Ocean carbon sink, Scientific reports, 9, 7384, https://doi.org/https://doi.org/10.1038/s41598-019-43826-y, 2019.

Lauvset, S. K., Key, R. M., Olsen, A., van Heuven, S., Velo, A., Lin, X., Schirnick, C., Kozyr, A., Tanhua, T., Hoppema, M., Jutterström, S., Steinfeldt, R., Jeansson, E., Ishii, M., Perez, F. F., Suzuki, T., and Watelet, S.: A New Global Interior Ocean Mapped Climatology: The $1^\circ x1^\circ$ GLODAP Version 2, Earth System Science Data, 8, 325–340, https://doi.org/10.5194/essd-8-325-2016, 2016.

Lauvset, S. K., Lange, N., Tanhua, T., Bittig, H. C., Olsen, A., Kozyr, A., Álvarez, M., Azetsu-Scott, K., Brown, P. J., Carter, B. R., Cotrim da Cunha, L., Hoppema, M., Humphreys, M. P., Ishii, M., Jeansson, E., Murata, A., Müller, J. D., Perez, F. F., Schirnick, C., Steinfeldt, R.,

https://doi.org/10.5194/egusphere-2024-1750
Preprint. Discussion started: 20 June 2024

Suzuki, T., Ulfsbo, A., Velo, A., Woosley, R. J., and Key, R.: The annual update GLODAPv2.2023: the global interior ocean biogeochemical data product, Earth System Science Data Discussions, 2024, 1–32, https://doi.org/10.5194/essd-2023-468, 2024a.

Lauvset, S. K., Lange, N., Tanhua, T., Bittig, H. C., Olsen, A., Kozyr, A., Álvarez, M., Azetsu-Scott, K., Brown, P. J., Carter, B. R., Cotrim da Cunha, L., Hoppema, M., Humphreys, M. P., Ishii, M., Jeansson, E., Murata, A., Müller, J. D., Pérez, F. F., Schirnick, C., Steinfeldt, R., Suzuki, T., Ulfsbo, A., Velo, A., Woosley, R. J., and Key, R. M.: The annual update GLODAPv2.2023: the global interior ocean biogeochemical data product, Earth System Science Data, 16, 2047–2072, https://doi.org/10.5194/essd-16-2047-2024, 2024b.

Le Quéré, C., Raupach, M. R., Canadell, J. G., Marland, G., Bopp, L., Ciais, P., Conway, T. J., Doney, S. C., Feely, R. A., Foster, P., Friedlingstein, P., Gurney, K., Houghton, R. A., House, J. I., Huntingford, C., Levy, P. E., Lomas, M. R., Majkut, J., Metzl, N., Ometto, J. P., Peters, G. P., Prentice, I. C., Randerson, J. T., Running, S. W., Sarmiento, J. L., Schuster, U., Sitch, S., Takahashi, T., Viovy, N., Van Der Werf, G. R., and Woodward, F. I.: Trends in the sources and sinks of carbon dioxide, Nature Geoscience, 2, 831–836, https://doi.org/10.1038/ngeo689, 2009.

Liao, E., Resplandy, L., Liu, J., and Bowman, K. W.: Amplification of the ocean carbon sink during El Niños: Role of poleward Ekman transport and influence on atmospheric CO2, Global Biogeochemical Cycles, 34, https://doi.org/10.1029/2020GB006574, 2020.

Long, M. C., Stephens, B. B., McKain, K., Sweeney, C., Keeling, R. F., Kort, E. A., Morgan, E. J., Bent, J. D., Chandra, N., Chevallier, F., Commane, R., Daube, B. C., Krummel, P. B., Loh, Z., Luijkx, I. T., Munro, D., Patra, P., Peters, W., Ramonet, M., Rödenbeck, C., Stavert, A., Tans, P., and Wofsy, S. C.: Strong Southern Ocean carbon uptake evident in airborne observations, Science, 374, 1275–1280, https://doi.org/10.1126/science.abi4355, 2021.

Mamnun, N., Völker, C., Krumscheid, S., Vrekoussis, M., and Nerger, L.: Global Sensitivity Analysis of a One-Dimensional Ocean Biogeochemical Model, Socio-Environmental Systems Modelling, 5, 18 613, https://doi.org/10.18174/sesmo.18613, 2023.

Mayot, N., Le Quéré, C., Rödenbeck, C., Bernardello, R., Bopp, L., Djeutchouang, L. M., Gehlen, M., Gregor, L., Gruber, N., Hauck, J., Iida, Y., Ilyina, T., Keeling, R. F., Landschü"tzer, P., Manning, A. C., Patara, L., Resplandy, L., Schwinger, J., Séférian, R., Watson, A. J., Wright, R. M., and Zeng, J.: Climate-driven variability of the Southern Ocean CO_2 sink, Philosophical Transactions of the Royal Society A: Mathematical, Physical and Engineering Sciences, 381, 20220 055, https://doi.org/10.1098/rsta.2022.0055, 2023.

Menemenlis, D., Fukumori, I., and Lee, T.: Using Green's Functions to Calibrate an Ocean General Circulation Model, Monthly Weather Review, 133, 1224–1240, https://doi.org/10.1175/MWR2912.1, 2005.

Mu, L., Nerger, L., Streffing, J., Tang, Q., Niraula, B., Zampieri, L., Loza, S. N., and Goessling, H. F.: Sea-Ice Forecasts With an Upgraded AWI Coupled Prediction System, Journal of Advances in Modeling Earth Systems, 14, e2022MS003 176, https://doi.org/10.1029/2022MS003176, 2022.

Müller, J. D., Gruber, N., Carter, B., Feely, R., Ishii, M., Lange, N., Lauvset, S. K., Murata, A., Olsen, A., Pérez, F. F., Sabine, C., Tanhua, T., Wanninkhof, R., and Zhu, D.: Decadal Trends in the Oceanic Storage of Anthropogenic Carbon From 1994 to 2014, AGU Advances, 4, e2023AV000 875, https://doi.org/10.1029/2023AV000875, 2023.

Nerger, L., Hiller, W., and Schröter, J.: PDAF - THE PARALLEL DATA ASSIMILATION FRAMEWORK: EXPERIENCES WITH KALMAN FILTERING, in: Use of High Performance Computing in Meteorology, pp. 63–83, WORLD SCIENTIFIC, Singapore, https://doi.org/10.1142/9789812701831_0006, 2005.

Nerger, L., Janjić, T., Schröter, J., and Hiller, W.: A Unification of Ensemble Square Root Kalman Filters, Monthly Weather Review, 140, 2335–2345, https://doi.org/10.1175/MWR-D-11-00102.1, 2012.

https://doi.org/10.5194/egusphere-2024-1750
Preprint. Discussion started: 20 June 2024

Nerger, L., Tang, Q., and Mu, L.: Efficient ensemble data assimilation for coupled models with the Parallel Data Assimilation Framework: example of AWI-CM (AWI-CM-PDAF 1.0), Geoscientific Model Development, 13, 4305–4321, https://doi.org/10.5194/gmd-13-4305-2020, 2020.

Nerger, L., Tang, Q., and Mu, L.: The PDAF model binding for AWI-CM (AWI-CM-PDAF version 1.0 update 1), https://doi.org/10.5281/zenodo.3822030, 2024.

Orr, J. C. and Epitalon, J.-M.: Improved routines to model the ocean carbonate system: mocsy 2.0, Geoscientific Model Development, 8, 485–499, https://doi.org/10.5194/gmd-8-485-2015, 2015.

Park, J.-Y., Stock, C. A., Yang, X., Dunne, J. P., Rosati, A., John, J., and Zhang, S.: Modeling global ocean biogeochemistry with physical data assimilation: a pragmatic solution to the equatorial instability, Journal of Advances in modeling earth systems, 10, 891–906, https://doi.org/10.1002/2017MS001223, 2018.

Pérez, F. F., Becker, M., Goris, N., Gehlen, M., López-Mozos, M., Tjiputra, J., Olsen, A., Müller, J. D., Huertas, I. E., Chau, T. T. T., Cainzos, V., Velo, A., Benard, G., Hauck, J., Gruber, N., and Wanninkhof, R.: An Assessment of CO2 Storage and Sea-Air Fluxes for the Atlantic Ocean and Mediterranean Sea Between 1985 and 2018, Global Biogeochemical Cycles, 38, e2023GB007 862, https://doi.org/10.1029/2023GB007862, 2024.

Peylin, P., Law, R. M., Gurney, K. R., Chevallier, F., Jacobson, A. R., Maki, T., Niwa, Y., Patra, P. K., Peters, W., Rayner, P. J., Rödenbeck, C., van der Laan-Luijkx, I. T., and Zhang, X.: Global atmospheric carbon budget: results from an ensemble of atmospheric CO2 inversions, Biogeosciences, 10, 6699–6720, https://doi.org/10.5194/bg-10-6699-2013, 2013.

Regnier, P., Resplandy, L., Najjar, R. G., and Ciais, P.: The land-to-ocean loops of the global carbon cycle, Nature, 603, 401–410, https://doi.org/10.1038/s41586-021-04339-9, 2022.

Rödenbeck, C., Bakker, D. C. E., Gruber, N., Iida, Y., Jacobson, A. R., Jones, S., Landschützer, P., Metzl, N., Nakaoka, S., Olsen, A., Park, G.-H., Peylin, P., Rodgers, K. B., Sasse, T. P., Schuster, U., Shutler, J. D., Valsala, V., Wanninkhof, R., and Zeng, J.: Data-based estimates of the ocean carbon sink variability – first results of the Surface Ocean pCO2 Mapping intercomparison (SOCOM), Biogeosciences, 12, 7251–7278, https://doi.org/10.5194/bg-12-7251-2015, 2015.

Sarmiento, J. L. and Gruber, N.: Carbon Cycle, in: Ocean Biogeochemical Dynamics, chap. 8, pp. 318–358, Princeton University Press, 2006.

Sathyendranath, S., Jackson, T., Brockmann, C., Brotas, V., Calton, B., Chuprin, A., Clements, O., Cipollini, P., Danne, O., Dingle, J., Donlon, C., Grant, M., Groom, S., Krasemann, H., Lavender, S., Mazeran, C., Mélin, F., Müller, D., Steinmetz, F., Valente, A., Zühlke, M., Feldman, G., Franz, B., Frouin, R., Werdell, J., and Platt, T.: ESA Ocean Colour Climate Change Initiative (Ocean_Colour_cci): Version 5.0 Data, NERC EDS Centre for Environmental Data Analysis, https://doi.org/10.5285/1dbe7a109c0244aaad713e078fd3059a, 2021.

Schartau, M., Engel, A., Schröter, J., Thoms, S., Völker, C., and Wolf-Gladrow, D.: Modelling carbon overconsumption and the formation of extracellular particulate organic carbon, Biogeosciences, 4, 433–454, https://doi.org/10.5194/bg-4-433-2007, 2007.

Scholz, P., Sidorenko, D., Gurses, O., Danilov, S., Koldunov, N., Wang, Q., Sein, D., Smolentseva, M., Rakowsky, N., and Jung, T.: Assessment of the Finite-volumE Sea ice-Ocean Model (FESOM2.0) – Part 1: Description of selected key model elements and comparison to its predecessor version, Geoscientific Model Development, 12, 4875–4899, https://doi.org/10.5194/gmd-12-4875-2019, 2019.

Scholz, P., Sidorenko, D., Danilov, S., Wang, Q., Koldunov, N., Sein, D., and Jung, T.: Assessment of the Finite-VolumE Sea ice–Ocean Model (FESOM2.0) – Part 2: Partial bottom cells, embedded sea ice and vertical mixing library CVMix, Geoscientific Model Development, 15, 335–363, https://doi.org/10.5194/gmd-15-335-2022, 2022.

https://doi.org/10.5194/egusphere-2024-1750
Preprint. Discussion started: 20 June 2024

Schourup-Kristensen, V., Sidorenko, D., Wolf-Gladrow, D. A., and Völker, C.: A Skill Assessment of the Biogeochemical Model REcoM2 coupled to the Finite Element Sea Ice Ocean Model (FESOM 1.3), Geoscientific Model Development, 7, 2769–2802, https://doi.org/10.5194/gmd-7-2769-2014, 2014.

Sidorenko, D.: The North Atlantic circulation derived from inverse models, Ph.D. thesis, University of Bremen, 2004.

Spring, A., Dunkl, I., Li, H., Brovkin, V., and Ilyina, T.: Trivial improvements in predictive skill due to direct reconstruction of the global carbon cycle, Earth System Dynamics, 12, 1139–1167, https://doi.org/10.5194/esd-12-1139-2021, 2021.

Stark, J., Donlon, C., Martin, M., and McCulloch, M.: OSTIA: An Operational, High Resolution, Real-Time, Global Sea Surface Temperature Analysis System, in: Oceans 07 IEEE Aberdeen, Conference Proceedings. Marine Challenges: Coastline to Deep Sea, IEEE, 2007.

Sutton, A. J., Williams, N. L., and Tilbrook, B.: Constraining Southern Ocean CO2 Flux Uncertainty Using Uncrewed Surface Vehicle Observations, Geophysical Research Letters, 48, e2020GL091 748, https://doi.org/10.1029/2020GL091748, 2021.

Takahashi, T., Olafsson, J., Goddard, J. G., Chipman, D. W., and Sutherland, S. C.: Seasonal variation of CO2 and nutrients in the high-latitude surface oceans: A comparative study, Global Biogeochemical Cycles, 7, 843–878, https://doi.org/10.1029/93GB02263, 1993.

Tang, Q., Mu, L., Sidorenko, D., Goessling, H., Semmler, T., and Nerger, L.: Improving the ocean and atmosphere in a coupled ocean–atmosphere model by assimilating satellite sea-surface temperature and subsurface profile data, Quarterly Journal of the Royal Meteorological Society, 146, 4014–4029, https://doi.org/10.1002/qj.3885, 2020.

Terhaar, J., Frölicher, T. L., and Joos, F.: Observation-constrained estimates of the global ocean carbon sink from Earth system models, Biogeosciences, 19, 4431–4457, https://doi.org/10.5194/bg-19-4431-2022, 2022.

Terhaar, J., Goris, N., Müller, J. D., DeVries, T., Gruber, N., Hauck, J., Perez, F. F., and Séférian, R.: Assessment of Global Ocean Biogeochemistry Models for Ocean Carbon Sink Estimates in RECCAP2 and Recommendations for Future Studies, Journal of Advances in Modeling Earth Systems, 16, e2023MS003 840, https://doi.org/10.1029/2023MS003840, 2024.

Tsujino, H., Urakawa, S., Nakano, H., Small, R. J., Kim, W. M., Yeager, S. G., Danabasoglu, G., Suzuki, T., Bamber, J. L., Bentsen, M., Böning, C. W., Bozec, A., Chassignet, E. P., Curchitser, E., Boeira Dias, F., Durack, P. J., Griffies, S. M., Harada, Y., Ilicak, M., Josey, S. A., Kobayashi, C., Kobayashi, S., Komuro, Y., Large, W. G., Le Sommer, J., Marsland, S. J., Masina, S., Scheinert, M., Tomita, H., Valdivieso, M., and Yamazaki, D.: JRA-55 based surface dataset for driving ocean–sea-ice models (JRA55-do), Ocean Modelling, 130, 79–139, https://doi.org/10.1016/j.ocemod.2018.07.002, 2018.

Verdy, A. and Mazloff, M. R.: A data assimilating model for estimating Southern Ocean biogeochemistry, Journal of Geophysical Research: Oceans, 122, 6968–6988, https://doi.org/10.1002/2016JC012650, 2017.

Vetra-Carvalho, S., van Leeuwen, P. J., Nerger, L., Barth, A., Altaf, M. U., Brasseur, P., Kirchgessner, P., and Beckers, J.-M.: State-of-the-art stochastic data assimilation methods for high-dimensional non-Gaussian problems, Tellus A: Dynamic Meteorology and Oceanography, 70, 1–43, https://doi.org/10.1080/16000870.2018.1445364, 2018.

Völker, C., Wallace, D. W. R., and Wolf-Gladrow, D. A.: On the role of heat fluxes in the uptake of anthropogenic carbon in the North Atlantic, Global Biogeochemical Cycles, 16, 85–1–85–9, https://doi.org/10.1029/2002GB001897, 2002.

Wanninkhof, R.: Relationship between wind speed and gas exchange over the ocean revisited, Limnology and Oceanography: Methods, 12, 351–362, https://doi.org/10.4319/lom.2014.12.351, 2014.

Wanninkhof, R., Park, G.-H., Takahashi, T., Sweeney, C., Feely, R., Nojiri, Y., Gruber, N., Doney, S. C., McKinley, G. A., Lenton, A., Le Quéré, C., Heinze, C., Schwinger, J., Graven, H., and Khatiwala, S.: Global ocean carbon uptake: magnitude, variability and trends, Biogeosciences, 10, 1983–2000, https://doi.org/10.5194/bg-10-1983-2013, 2013.

https://doi.org/10.5194/egusphere-2024-1750
Preprint. Discussion started: 20 June 2024

Williams, N. L., Juranek, L. W., Feely, R. A., Johnson, K. S., Sarmiento, J. L., Talley, L. D., Dickson, A. G., Gray, A. R., Wanninkhof, R., Russell, J. L., Riser, S. C., and Takeshita, Y.: Calculating surface ocean pCO2 from biogeochemical Argo floats equipped with pH: An uncertainty analysis, Global Biogeochemical Cycles, 31, 591–604, https://doi.org/10.1002/2016GB005541, 2017.

Wunsch, C.: The Ocean Circulation Inverse Problem, Cambridge University Press, Cambridge, England, UK, https://doi.org/10.1017/CBO9780511629570, 1996.